Cellular and Molecular Life Sciences (2024) 81:102
https://doi.org/10.1007/s00018-024-05132-3

ORIGINAL ARTICLE

Pathological mutations reveal the key role of the cytosolic iRhom2 N-terminus for phosphorylation-independent 14-3-3 interaction and ADAM17 binding, stability, and activity

Katharina Bläsius[1] · Lena Ludwig[1] · Sarah Knapp[2] · Charlotte Flaßhove[1] · Friederike Sonnabend[1] · Diandra Keller[1] · Nikola Tacken[1] · Xintong Gao[1] · Selcan Kahveci-Türköz[1] · Caroline Grannemann[1] · Aaron Babendreyer[1] · Colin Adrain[3] · Sebastian Huth[4] · Jens Malte Baron[4] · Andreas Ludwig[1] · Stefan Düsterhöft[1]

Received: 29 November 2023 / Accepted: 15 January 2024
© The Author(s) 2024

Abstract

The protease ADAM17 plays an important role in inflammation and cancer and is regulated by iRhom2. Mutations in the cytosolic N-terminus of human iRhom2 cause tylosis with oesophageal cancer (TOC). In mice, partial deletion of the N-terminus results in a curly hair phenotype (cub). These pathological consequences are consistent with our findings that iRhom2 is highly expressed in keratinocytes and in oesophageal cancer. Cub and TOC are associated with hyperactivation of ADAM17-dependent EGFR signalling. However, the underlying molecular mechanisms are not understood. We have identified a non-canonical, phosphorylation-independent 14-3-3 interaction site that encompasses all known TOC mutations. Disruption of this site dysregulates ADAM17 activity. The larger cub deletion also includes the TOC site and thus also dysregulated ADAM17 activity. The cub deletion, but not the TOC mutation, also causes severe reductions in stimulated shedding, binding, and stability of ADAM17, demonstrating the presence of additional regulatory sites in the N-terminus of iRhom2. Overall, this study contrasts the TOC and cub mutations, illustrates their different molecular consequences, and reveals important key functions of the iRhom2 N-terminus in regulating ADAM17.

Keywords Esophageal squamous cancer · Ectodomain shedding · EGFR ligand release · Curly-bare (cub) mouse · iRhom2 · ADAM17 · Howel–Evans syndrome · Tylosis with oesophageal cancer (TOC) · 14-3-3 proteins · Stratifin

Abbreviations

ADAM	A disintegrin and metalloproteinases
AREG	Amphiregulin
coIP	Co-Immunoprecipitation
EGFR	Epidermal growth factor receptor
FRMD8	FERM domain containing 8
IFN	Interferon
IL	Interleukin
IL1R2	Interleukin 1 receptor 2
IDR	Intrinsically disordered region
IRHD	IRhom homology domain
OC	Oesophageal cancer
OAC	Oesophageal adenocarcinoma
OSCC	Oesophageal squamous cell carcinoma
PAE	Predicted aligned error
pLDDT	Predicted local distance difference test
TGFα	Transforming growth factor alpha
TNFα	Tumour necrosis factor alpha

Katharina Bläsius and Lena Ludwig contributed equally to this work.

✉ Stefan Düsterhöft
sduesterhoeft@ukaachen.de

[1] Institute of Molecular Pharmacology, Medical Faculty, RWTH Aachen University, Wendlingweg 2, 52074 Aachen, Germany

[2] Institute of Biochemistry and Molecular Biology, Medical Faculty, RWTH Aachen University, Aachen, Germany

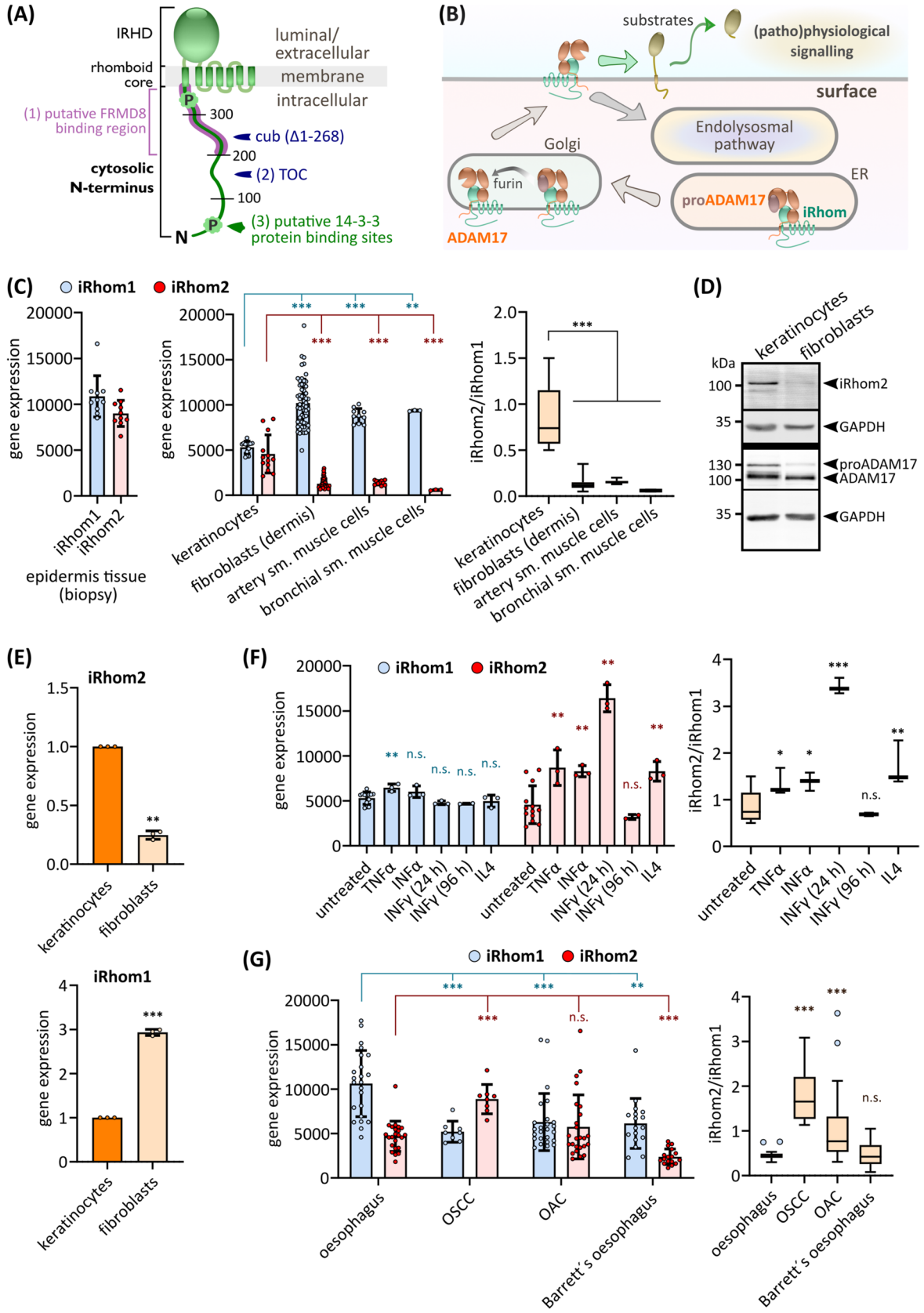
[3] Patrick G Johnston Centre for Cancer Research, Queen's University, Belfast, Northern Ireland

[4] Department of Dermatology and Allergology, Medical Faculty, RWTH Aachen University, Aachen, Germany

Introduction

Oesophageal cancer (OC) is a critical global health concern, given its alarming prognosis and high mortality rate, ranking as the sixth leading cause of cancer-related

Published online: 27 February 2024


(A)
IRHD
rhomboid core
(1) putative FRMD8 binding region
cytosolic N-terminus
luminal/ extracellular
membrane
intracellular
P
300
cub (Δ1-268)
200
(2) TOC
100
P
N
(3) putative 14-3-3 protein binding sites
(B)
substrates
(patho)physiological signalling
surface
Endolysosmal pathway
Golgi
furin
ER
proADAM17
iRhom
ADAM17
(C)
iRhom1
iRhom2
gene expression
iRhom2/iRhom1
epidermis tissue (biopsy)
keratinocytes
fibroblasts (dermis)
artery sm. muscle cells
bronchial sm. muscle cells
(D)
kDa
keratinocytes
fibroblasts
iRhom2
GAPDH
proADAM17
ADAM17
(E)
iRhom2
iRhom1
gene expression
keratinocytes
fibroblasts
(F)
untreated
TNFα
INFα
INFγ (24 h)
INFγ (96 h)
IL4
n.s.
(G)
oesophagus
OSCC
OAC
Barrett´s oesophagus

◂**Fig. 1** iRhom2 gene expression is high in skin and OSCC. **A** Structurally, iRhoms have a distinct topology composed of a rhomboid core with seven transmembrane helices (TMH). The extracellular iRhom homology domain (IRHD) is situated between TMH1 and TMH2. Additionally, iRhoms possess a large cytosolic N-terminal elongation: 375 residues in murine iRhom2 and 403 residues in human iRhom2. Relative positions of key characteristics are labelled for murine iRhom2: (1) putative FRMD8 binding site; (2) TOC mutation site—in human iRhom2: I186T (murine position: 156) [12], D188N (murine position: 158) [12], D188Y (murine position: 158) [72], P189L (murine position: 159) [12], R197S (murine position: 167) [83]; (3) phosphorylation sites and putative 14-3-3 binding sites. **B** Role of iRhoms in ADAM17 biology: iRhoms regulate ADAM17 by binding to proADAM17 in the ER and transporting it to the Golgi for maturation. The inhibitory prodomain is then proteolytically removed by furin-like proteases. This process allows ADAM17 in complex with iRhoms to localise to the cell surface and initiate shedding of its substrates, enabling various pathways including TNFα and EGFR signalling. **C** Curated Affymetrix Human Genome U133 Plus 2.0 Array platform data from public repositories [44] were assessed with the GENEVESTIGATOR software. The GENEVESTIGATOR platform allows for the comparison of mRNA expression of genes between samples of different experimental data sets: Gene expression levels of iRhom1 and iRhom2 from healthy human epidermis tissue ($n=10$), untreated primary human keratinocytes from healthy tissue ($n=13$), untreated primary human fibroblasts from healthy dermis tissue ($n=57$), untreated primary human artery smooth muscle cells from healthy heart tissue ($n=10$), untreated primary human bronchial smooth muscle cells from healthy heart tissue ($n=10$) were analysed. To compare the gene expression levels of iRhom1 and iRhom2 in one sample, the iRhom2/iRhom1 ratio was calculate for each sample. **D** Immunoblot of cell lysates from primary keratinocytes or primary fibroblasts. $n=3$. **E** RT-qPCR of primary keratinocytes and primary fibroblasts. $n=3$. **F, G** Data from curated Affymetrix Human Genome U133 Plus 2.0 Array platform data as described in (**C**): **F** Gene expression levels of iRhom1 and iRhom2 in primary keratinocytes from healthy tissue treated with: untreated control ($n=13$) or treated for 24 h with indicated proinflammatory stimulants ($n=3$) or treated for 96 h with IFNγ ($n=2$). **G** Gene expression levels of iRhom1 and iRhom2 in healthy human oesophagus squamous tissue ($n=23$) compared to expression levels in human oesophageal squamous cell carcinoma (OSCC; $n=8$), human oesophageal adenocarcinoma (OAC; $n=26$) and Barrett´s oesophagus ($n=17$)

death worldwide. Oesophageal squamous cell carcinoma (OSCC) and oesophageal adenocarcinoma (OAC) are the primary histological subtypes of OC. Despite their similarities, OSCC and OAC differ both epidemiologically and biologically [87, 103, 109]. The prognosis for OSCC, which comprises most OC cases, is exceptionally poor [109, 119]. Notably, smoking and alcohol consumption serve as significant risk factors for OSCC development. However, the underlying molecular and genetic mechanisms driving OC remain poorly understood.

Howel-Evans syndrome, also called tylosis with oesophageal carcinoma (TOC), directly correlates with an increased risk to develop OSCC [12, 43]. This rare genetic disorder affects the seven-transmembrane spanning pseudoprotease iRhom2 (Fig. 1A) and its functions, altering EGF receptor (EGFR) signalling pathways by aggravating iRhom2-dependent ectodomain shedding [12].

Shedding, the proteolytic release of ectodomains from membrane proteins, is a crucial mechanism in many physiological and pathological processes. The released soluble ectodomains, which are often receptors or receptor ligands, exhibit potent biological activity. iRhoms, pseudoproteases of the rhomboid family, play a crucial role in the shedding process by forming a complex with the transmembrane sheddase ADAM17 (A-disintegrin and metalloproteinase 17) [19, 59, 100, 101].

ADAM17 has a broad spectrum of substrates, including cytokines, growth factors and cytokine receptors such as tumour necrosis factor (TNF) [10], transforming growth factor α (TGFα) and amphiregulin (AREG) [80, 92]. Release of these substrates is crucially involved in various (patho-) physiological processes [11, 80] highlighting the central role of ADAM17 in development and in the immune response but also in chronic inflammation and cancer. Additionally, the multi-faceted role of ADAM17 in virus entry has been recently demonstrated [47, 56, 75, 79, 120, 123].

The formation of the iRhom-ADAM17 complex is a necessary step for ADAM17 maturation (Fig. 1A, B) [19, 24, 34, 50, 65]. On the cell surface, the shedding activity of ADAM17 is further regulated by iRhoms [16, 34]. In mammals, two genes for iRhoms exist: RHBDF1 (iRhom1) and RHBDF2 (iRhom2). While iRhom1 is present in most cell types, iRhom2 initially appeared to be immune cell specific but is also upregulated during inflammatory episodes in other cell lineages such as endothelial and epithelial cells [8, 33, 61]. Consistent with this, iRhom2 deficiency in mice and humans does not cause obvious developmental defects but impairs the immune response [2, 54, 67].

iRhoms contain a large N-terminal cytosolic elongation that has not yet been fully characterised (Fig. 1A). The genetic disorder causing TOC is caused by single point mutations in the N-terminus [12, 27, 28, 43, 72, 91]. This disorder is characterised by symptoms such as leukoplakia and hyperkeratosis and increases the risk of OSCC [17]. The mutations are classified as "gain of function" because they apparently upregulate ADAM17 activity, resulting in higher levels of EGFR ligands, EGFR hyperactivation in keratinocytes and increased release of TNF receptor 1, leading to reduced apoptosis [12, 40, 63].

In mice, a spontaneous mutation called cub (curly-bare) results in a deletion of 268 amino acid residues of the N-terminus including the TOC mutation positions, causing aberrant hair growth, hyperkeratosis and hyperproliferative wound healing [39, 48, 100]. This cub deletion was linked to higher ADAM17-mediated shedding of AREG. Likewise, different studies contested the notion that the cub mutation results in higher ADAM17 activity at least in in vitro settings [39, 100]. Interestingly, mice carrying TOC mutations exhibit the same skin-related phenotype as cub mice [39, 40, 42]. Noteworthy, the deficiency in iRhom2 in mice seems to

cause a thinning of the epidermis in the footpad [66]. The phenotype of both, cub and TOC mice, can be rescued by AREG deficiency, suggesting a similar underlying process with increased AREG-dependent signalling [40]. However, the molecular mechanism for these mutations remains unknown.

Only a few regulatory regions have been identified within the N-terminus of iRhom2, including phosphorylation sites that facilitate phosphorylation-dependent binding of members of the 14-3-3 protein family [16, 34]. Deletion of the entire N-terminus appears to destabilise the iRhom-ADAM17 complex, resulting in the loss of matured ADAM17. The adapter protein FRMD8, also known as iTAP (iRhom tail-associated protein) has been identified as an essential binding partner of the N-terminus of iRhom, which has a stabilising function for iRhom and thus for the iRhom-ADAM17 complex [55, 77]. This seems to explain the loss of ADAM17 when the N-terminus is missing. Notably, part of this FRMD8-binding region is lost in the cub deletion, while the TOC mutations lie outside this region. Recently, it was shown that the N-terminus is cleaved off by a signal peptidase complex and migrates to the nucleus, where it influences gene expression [23, 122].

In this study, we observed high expression levels of iRhom2 in skin tissue samples and primary keratinocytes under physiological conditions, providing an explanation for the distinct skin-related phenotype in humans and mice with TOC or cub, respectively. Notably, iRhom2 and ADAM17 expression levels were significantly upregulated in OSCC patient samples, which is consistent with the higher risk for OSCC in TOC patients.

It is important to separate the direct molecular effects of both mutation types (single point mutation vs large deletion) on the functions of the iRhom2-ADAM17 complex from downstream effects: In vivo, altered ADAM17 activity and the mutated soluble iRhom2 N-terminus in the nucleus will have long-term effects on gene expression as well as ADAM17-dependent signalling pathways. Here, we focused on the direct molecular consequences of the TOC single-point mutations and the large cub deletion. We identified a highly conserved motif that contains all known TOC sites and represents a phosphorylation-independent 14-3-3 protein interaction site. Disruption of this site results in loss of regulation of ADAM17 activity, leading to increased constitutive shedding. In contrast, the pathological murine cub deletion covers a larger part of the N-terminus, including the TOC site. The cub deletion loses the ability to promote stimulated/activatable ADAM17 activity. In addition, we found that this deletion decreases binding to ADAM17 and causes accelerated degradation of ADAM17.

Overall, our results provide deeper insights into the molecular mechanisms controlling the iRhom2-ADAM17 complex through the N-terminus of iRhom2 by demonstrating a distinct effect of TOC site disruption, in contrast to the multiple overlapping and therefore more severe effects of the cub deletion.

Results

iRhom2 expression levels are high in skin and OSCC

The observed phenotypes of iRhom2 deficiency and cub deletion, as well as the pathologies associated with the human TOC mutations, clearly point to a central role of iRhom2 in epidermal tissue. While high iRhom2 expression is often primarily associated with immune cells, its expression pattern in the epidermis is not yet well defined. Hence, we analysed gene expression data from skin biopsies of healthy individuals obtained from publicly available microarray data [44]. We indeed observed a robust expression of iRhom2 in the skin samples (Fig. 1C). Moreover, primary human keratinocytes have significantly higher levels of iRhom2 expression compared to primary fibroblasts, artery smooth muscle cells, and bronchial smooth muscle cells (Fig. 1C). Notably, the ratio of iRhom2 to iRhom1 is substantially higher in keratinocytes than in other primary cell types (Fig. 1C, Fig. S1A), indicating a pivotal role for iRhom2 in regulating ADAM17 activity in keratinocytes in vivo. To verify the microarray data, we analysed iRhom1 and iRhom2 protein levels via immunoblotting and gene expression via RT-qPCR in primary keratinocytes and fibroblasts. Indeed, in agreement with the microarray data, we found higher protein levels and gene expression of iRhom2 in keratinocytes compared to fibroblasts (Fig. 1D, E). This expression pattern aligns with the predominantly skin-related manifestations of TOC and cub. We found a similar pattern in murine primary keratinocytes, again highlighting iRhom2's importance in regulating ADAM17 activity in the skin (Fig. S1B).

Considering the known induction of iRhom2 expression in response to proinflammatory stimuli [8, 33], we investigated whether the observed iRhom2 expression patterns in primary keratinocytes were due to pre-activation by proinflammatory conditions. We found a significant increase in iRhom2 gene expression in primary keratinocytes 24 h after treatment with proinflammatory stimuli, while iRhom1 showed no such elevation (Fig. 1F). This finding supports that the high iRhom2 expression in primary keratinocytes is likely the basal level under physiological conditions which can be further increased under inflammatory conditions. Furthermore, the gene expression pattern of untreated keratinocytes is also consistent with the basal iRhom2 and iRhom1 gene expression pattern in healthy human skin biopsies (Fig. 1C).

Since TOC mutations also pose an increased risk of developing OSCC, we examined iRhom2 expression in OSCC samples and compared them to healthy oesophagus squamous tissue, as well as samples from OAC and a pre-malignant condition, called Barrett's oesophagus. In OSCC samples, we observed a significant upregulation of iRhom2, accompanied by a downregulation of iRhom1, compared to healthy oesophagus squamous tissue (Fig. 1G). The ratio of iRhom2 to iRhom1 was four times higher in OSCC samples than in the healthy tissue. While OAC samples also showed a significantly elevated iRhom2-iRhom1 ratio, the increase was less pronounced (Fig. 1G). On the other hand, samples from Barrett's oesophagus exhibited no change in the ratio but displayed an overall reduction in iRhom1 and iRhom2 gene expression. Furthermore, we found a significant upregulation of ADAM17 gene expression exclusively in OSCC samples (Fig. S1C). In contrast, ADAM10, a close relative of ADAM17 with a partially overlapping substrate spectrum and independent of iRhom functions, did not show this expression pattern (Fig. S1C). The gene expression of EGFR ligands, TGFα and AREG, crucial ADAM17 substrates, did not show significant changes in OSCC compared to healthy tissue (Fig. S1C). To ensure that the elevated levels of iRhom2 in OSCC were not due to persistent proinflammatory conditions or the presence of tumour microenvironment-associated immune cells, we examined proinflammatory markers and immune cell markers. We observed no significantly elevated gene expression of TNF or IL6 (Fig. S1C), and only minimal gene expression of CD14, suggesting the presence of some monocytes/macrophages in the samples but not in sufficient quantities to explain the high iRhom2 levels in OSCC (Fig. S1D, S2A,B).

In summary, the gene expression patterns of iRhom2 and ADAM17 support the notion of an important role for iRhom2-dependent ADAM17 activity in both skin and OSCC, which is consistent with the pathological consequences of TOC single point mutations and cub deletion.

The N-terminal elongation represents a large intrinsically disordered part of iRhom2

To investigate the molecular mechanisms underlying the functions of the cytosolic N-terminal elongation of iRhom2, we performed in silico structural studies. Our bioinformatic analyses predict that the N-terminal elongation of iRhom2 has a largely unstructured/intrinsically disordered nature (Fig. 2A), which is typical for protein–protein interaction interfaces [5, 26]. Using the A.I.-based AlphaFold2 algorithm, we predicted the structural makeup of the N-terminus, which revealed an overall low pLDDT and PAE, again confirming a lack of higher structural regions (Fig. 2B–D). Some isolated secondary structures were predicted, but the N-terminus seems to be primarily intrinsically disordered (Fig. 2A–F), which is a hallmark to promote protein–protein interaction.

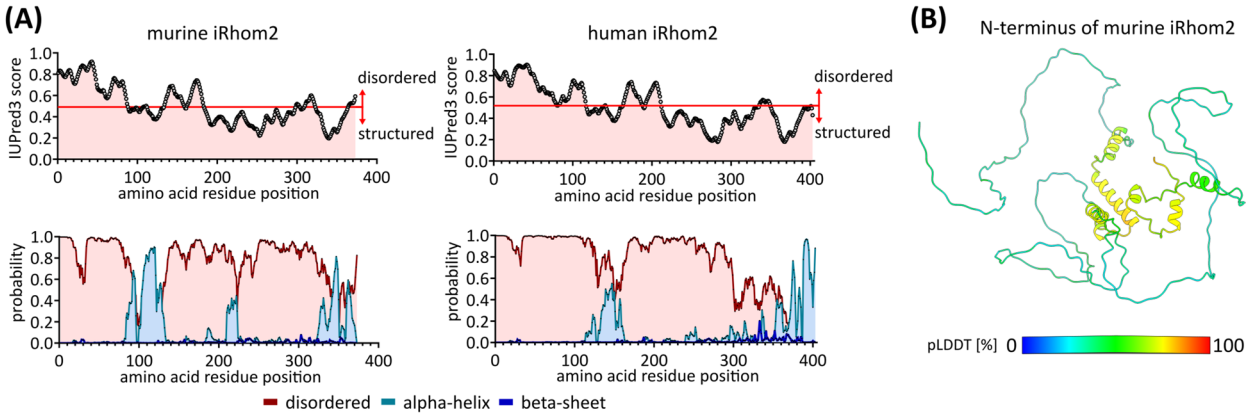
However, while the N-terminus seems to play a crucial role in regulating the iRhom-ADAM17 complex, only a handful of direct interactors such as FRMD8, ERK2, and 14-3-3 proteins have been identified (Fig. 1A) [16, 34, 55, 77, 95]. Using ANCHOR2, we have identified an additional region that is highly likely to be an interface for protein–protein interactions (Fig. 2E). Strikingly, this region is highly conserved and includes all known TOC mutation positions (Fig. 2E, F). In addition, R192 in the middle of this TOC site was found to be methylated in human iRhom2 by three independent high-throughput proteomic screens (Fig. 2F) [35, 38]. This further supports the TOC site as a regulatory interaction site, as protein methylation is a hallmark of protein interaction sites.

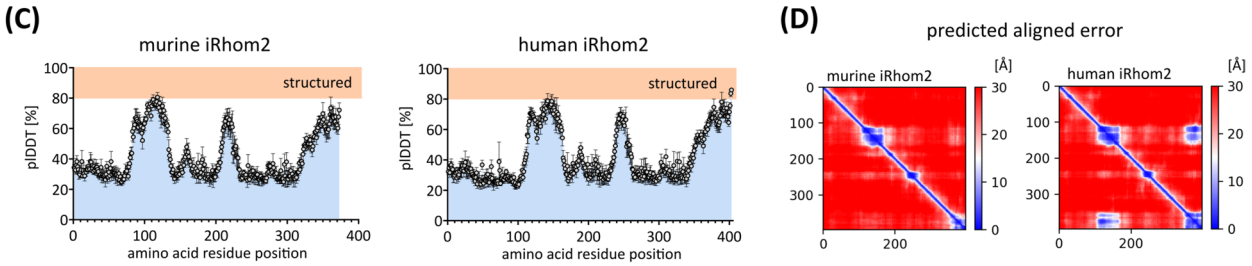
Furthermore, our bioinformatic analysis of the N-terminus of iRhom2 also indicates the presence of a nuclear localisation sequence (NLS), which is consistent with recent observations of its translocation to the nucleus after cleavage by the signal peptidase complex (Fig. 2G) [23].

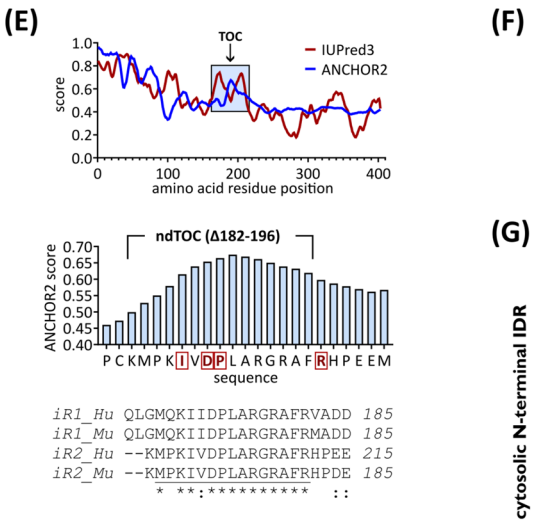
Overall, the N-terminal elongation represents a large intrinsically disordered region (IDR) that provides distinct hubs for regulation and interaction. Furthermore, all known TOC mutations are part of a predicted protein–protein interaction site.

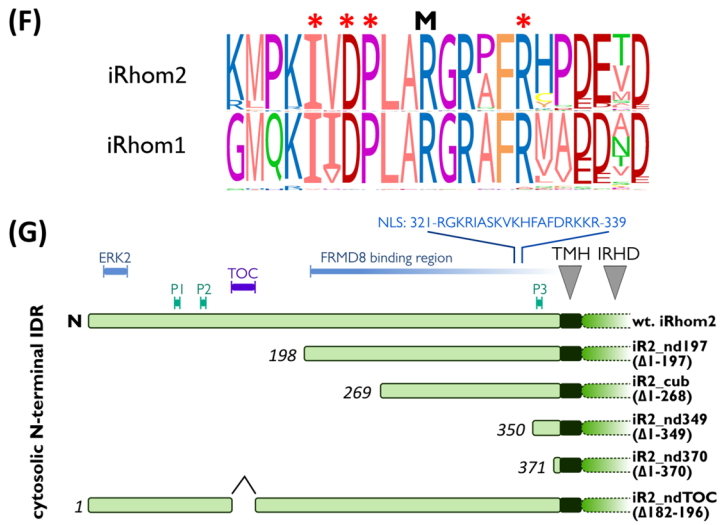
The TOC mutations and the cub deletion result in distinct molecular consequences for ADAM17

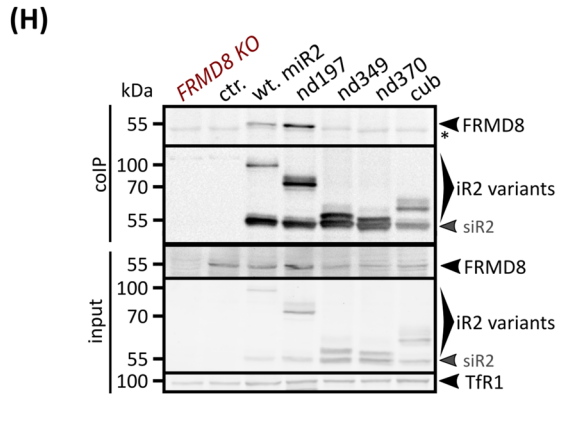
To gain a comprehensive understanding of the regulatory system acting on the iRhom2-ADAM17 complex, it is important to understand the molecular similarities and differences between the TOC single point mutations and cub deletions, as they exhibit a strikingly similar phenotype in mice [40]. While the TOC mutations affect a distinct region, the cub deletion affects a large part of the N-terminal IDR encompassing different known regulatory and interaction sites such as two phosphorylation sites, the TOC region as well as the ERK2 binding site (Fig. 2G). The exact binding site of the FRMD8 interaction is not yet known, but the approximate binding region was mapped before (Fig. 2G) [55, 77]. Hence, in contrast to TOC mutations the cub deletion affects most likely more regulatory aspects. To further dissect the molecular regulations of iRhom2 and its dysregulation, we designed an additional N-terminal deletion (nd197) that still contains the FRMD8 binding region and therefore retains binding to endogenous FRMD8 (Fig. 2G, H). In contrast, we could not detect FRMD8 binding for the cub deletion. We created two additional deletions (nd349 and nd370) with almost the entire N-terminus removed (Fig. 2G, H) to compare the effect of complete loss of the cytosolic N-terminal IDR with

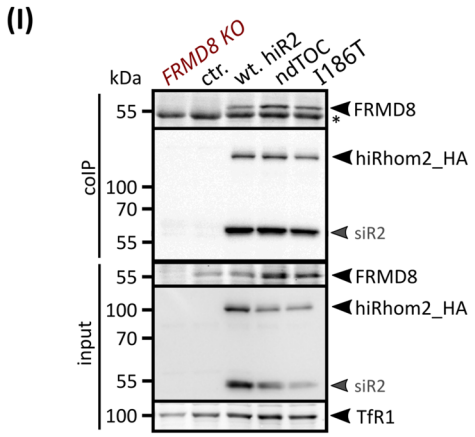

(A)
murine iRhom2
human iRhom2
IUPred3 score
disordered
structured
amino acid residue position
probability
disordered
alpha-helix
beta-sheet
(B)
N-terminus of murine iRhom2
pLDDT [%] 0 100


(C)
murine iRhom2
human iRhom2
pIDDT [%]
structured
amino acid residue position
(D)
predicted aligned error
murine iRhom2
human iRhom2
[Å]


(E)
TOC
IUPred3
ANCHOR2
score
amino acid residue position
ndTOC (Δ182-196)
ANCHOR2 score
P C K M P K I V D P L A R G R A F R H P E E M
sequence
iR1_Hu QLGMQKIIDPLARGRAFRVADD 185
iR1_Mu QLGMQKIIDPLARGRAFRMADD 185
iR2_Hu --KMPKIVDPLARGRAFRHPEE 215
iR2_Mu --KMPKIVDPLARGRAFRHPDE 185


(F)
iRhom2
iRhom1
(G)
NLS: 321-RGKRIASKVKHFAFDRKKR-339
ERK2
TOC
FRMD8 binding region
TMH
IRHD
P1
P2
P3
N
cytosolic N-terminal IDR
wt. iRhom2
198
iR2_nd197 (Δ1-197)
269
iR2_cub (Δ1-268)
350
iR2_nd349 (Δ1-349)
371
iR2_nd370 (Δ1-370)
1
iR2_ndTOC (Δ182-196)


(H)
kDa
FRMD8 KO
ctr.
wt. miR2
nd197
nd349
nd370
cub
coIP
input
FRMD8
iR2 variants
siR2
TfR1


(I)
kDa
FRMD8 KO
ctr.
wt. hiR2
ndTOC
I186T
coIP
input
FRMD8
hiRhom2_HA
siR2
TfR1

◂**Fig. 2** The cytosolic N-terminal elongation of iRhom2 is an intrinsically disordered hub for regulation and differentially controls levels of ADAM17. **A** Using IUPred3 [29, 70] and NetSurfP-2.0 [52], we assessed the probability of disordered regions and the presence of different structural elements in the cytosolic N-terminus of murine and human iRhom2 (residue 1 to 375). IUPred3 score describes the probability of disordered regions. NetSurfP-2.0 output gives the probability of the presence of disorder, alpha-helices, and beta-sheets. **B** Ab initio structural modelling of the N-terminus of murine iRhom2 using the deep learning algorithm AlphaFold2. Best ranked model is depicted in cartoon representation coloured according to pLDDT (predicted local distance difference test in [%]) score. **C** Consistent with (**A**), the structural prediction of the N-terminus of murine and human iRhom2 using AlphaFold2 demonstrates only small locally structured regions: Hence the iRhom2 N-terminus is largely disordered, as indicated by the overall low average pLDDT score per sequence position of the five predicted, ranked models. **D** The predicted align error (PAE) of the best-ranked structural models supports this finding: the individual amino acid residues in the disordered/unstructured N-terminus are largely not fixed in their position relative to each other and therefore have a high spatial uncertainty (20–30 Å). **E** Using the bioinformatic tools IUPred3 and ANCHOR2 (Mészáros et al. 2009) putative binding sites within the cytoplasmic N-terminus of human iRhom2 were identified. The plots show the calculated probability for an amino acid residue to be part of a binding site. Regions above 50% probability (ANCHOR2) and with a certain length are putative binding sites such as the highly conserved region which harbours all known TOC mutations. Our designed TOC site deletion ndTOC comprises the three main TOC mutations, but not the newest identified R197S [83]. **F** We used the algorithm CONYAR [50] to retrieve all available amino acid sequences of iRhom1 and iRhom2 from UniProtKB and compare them to identify highly conserved regions within the amino acid sequences of that gene. In the case of iRhom2 (query: RHBDF2) sequences from 381 species and in the case of iRhom1 (query: RHBDF1) sequences of 301 species were extracted. The TOC site was identified by CONYAR as a highly conserved region and its conservation is shown as WebLogo representation. Asterisks indicate the positions of the natural occurring TOC mutations in human iRhom2. M indicates the position of arginine methylation found by high throughput proteomics [38]. **G** Overview of the relative position of key regulatory sites and binding interfaces in wt-iRhom2 and in our designed N-terminal deletions. Phosphorylation sites (P1, P2 and P3) are binding sites for 14-3-3 proteins. NLS: predicted nuclear localisation sequence. **H,I** To analyse binding between iRhom2 constructs and endogenous FRMD8, coIPs were performed using the indicated iRhom2 constructs (with HA tag) as bait. HEK293 cells stably expressing the indicated murine iRhom2 deletions (H) or human iRhom2 constructs (I) as well as GFP (ctr.) as negative control were used. At around 55 kDa the shorter fragment of cleaved iRhom2 (siR2) as reported before [2, 19] is visible. This fragment was described as consequence of cleavage by signal peptidase complex [23, 122] but may additionally occur as artefact after lysis as we detect inconsistent amounts of the small fragment in different experiments. $n = 4$

the partial deletions. We also hypothesised that the TOC single point mutations only gradually affect the function of the identified TOC site (Fig. 2E). Hence, we designed the deletion ndTOC (Δ182-192) to remove most of the TOC site (Fig. 2E, F). As expected, binding to FRMD8 in iRhom2 is not altered by either the TOC point mutation (I186T) or the deletion of the TOC site (ndTOC) compared to wt-iRhom2 (Fig. 2I).

The TOC mutations are autosomal dominant and the cub deletion leads to a phenotype already in heterozygosity. To analyse the direct molecular effects of these iRhom2 variants on ADAM17 regulation in combination with wt-iRhoms, we used HEK293 cells with endogenous iRhom1 and iRhom2 (Fig. S1E) as an already established and widely used model system [16, 50, 98], with epithelial morphology [45]. We used the pMOWS plasmid system with a low level of protein expression to most closely mimic endogenous levels, as we have done before [24, 50].

As iRhom levels are a rate-limiting factor for forward transport and maturation of ADAM17, increased expression of either human or murine wt-iRhom2 results in more matured ADAM17 (Fig. 3A–C), as shown before [24, 50]. Consequently, the amount of ADAM17 on the cell surface is also elevated (Fig. 3D, E). In contrast, expression of the murine iRhom2 cub deletion does not promote higher levels of matured ADAM17 (Fig. 3A), which is in line with recent in vivo findings [84]. Furthermore, the three deletions nd197, nd349 and nd370 showed also a significant decrease in matured ADAM17 levels compared to wt-iRhom2 (Fig. 3B). We also observed a significant reduction in total ADAM17 levels in cells expressing these deletions compared to wt-iRhom2 or the negative control (Fig. 3A, B). In line with these findings, the amount of ADAM17 on the surface was also lower in cells expressing the deletions compared to both wt-iRhom2 and even control cells (Fig. 3D), although the deletion constructs can be detected on the cell surface similarly to wt-iRhom2 (Fig. S3B). Notably, these effects seem to be FRMD8 independent since nd197 still binds endogenous FRMD8 (Fig. 2H).

Expression of iRhom2 with a human TOC mutation (I186T) or a deletion of the TOC site (ndTOC) also shows a reduced amount of matured ADAM17 compared to wt-iRhom2 (Fig. 3C). ndTOC seems to lead to an even stronger reduction than the single point mutation, suggesting that the complete deletion of the TOC site has a stronger effect than the single point mutation (Fig. 3C). However, in contrast to the larger deletions (nd187, cub, nd349 and nd379), we did not observe a reduction in the total amount of ADAM17 (Fig. 3C). Both iRhom2_I186T and ndTOC exhibit a cell surface presence similar to that of the wt-iRhom2 (Fig. S3C). iRhom2_I186T leads to increased ADAM17 surface localisation compared to control cells and the impact on surface ADAM17 levels is not significantly different to cells with wt-iRhom2 expression (Fig. 3E). Remarkably, ndTOC expression results in significantly lower levels of surface ADAM17 compared to wt-iRhom2 (Fig. 3E).

These findings demonstrate the importance of the cytosolic iRhom2 N-terminus in regulating ADAM17 functions. They highlight the differential effects of TOC mutations and the cub deletion on iRhom2 function and their substantial impact on ADAM17 maturation, surface localisation and

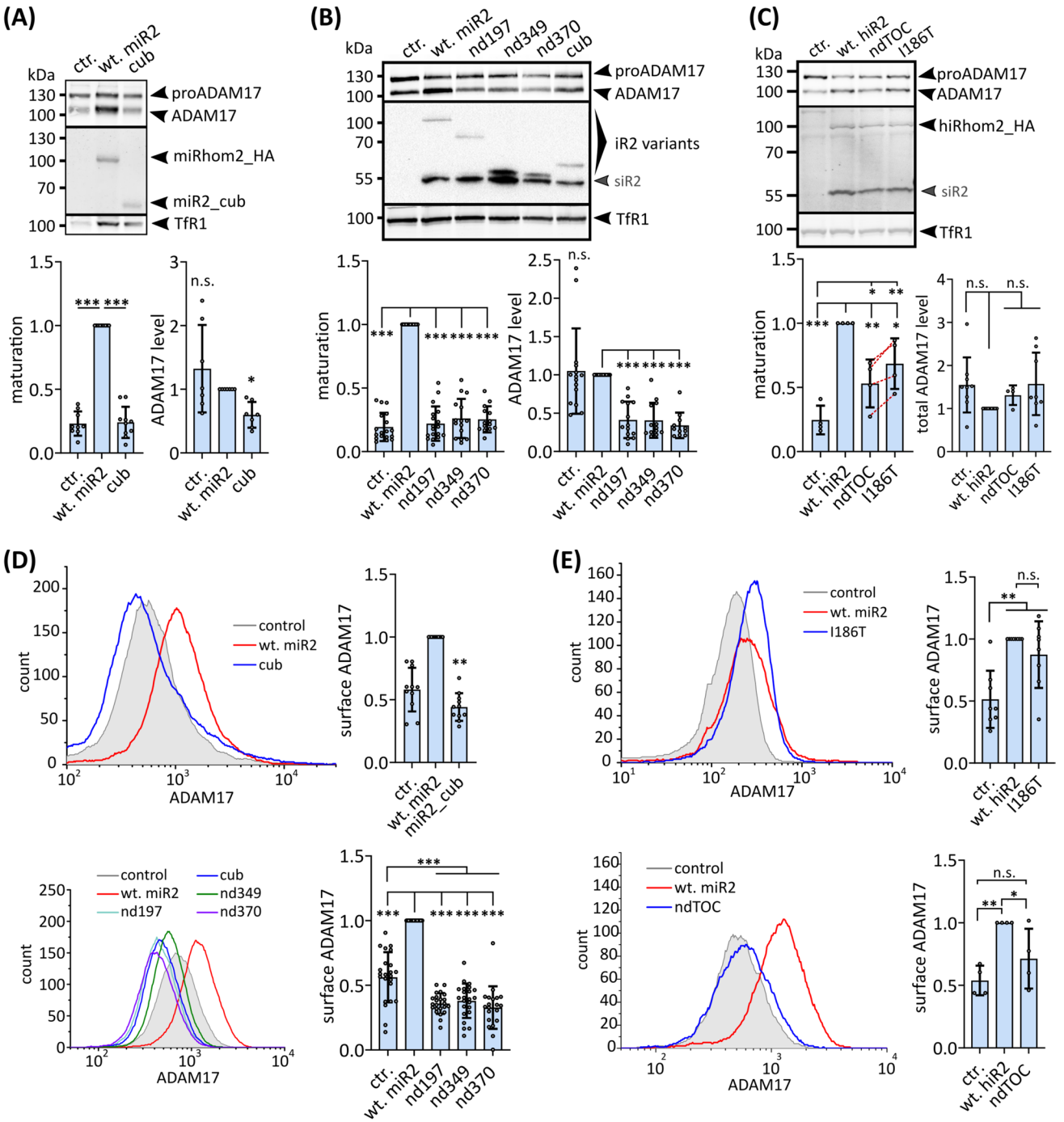


Fig. 3 The iRhom2 N-terminus regulates ADAM17 levels. **A–C** Immunoblot of samples from HEK293 cells stably expressing the indicated murine iRhom2 variants (A,B) or human iRhom2 variants (C) as well as GFP (ctr.) as negative control. Glycosylated proteins from cell lysates were enriched with concanavalin A beads. HEK293 cells have endogenous iRhoms and therefore exhibit a basal level of ADAM17 maturation. The maturation level of ADAM17 can be detected by the presence of matured ADAM17 with a lower molecular weight than proADAM17. ADAM17 maturation was assessed by densitometric measurements and calculation of the ratio between ADAM17 and proADAM17. Total ADAM17 levels were assessed by densitometric measurements and calculation of the ratio between total ADAM17 (ADAM17 plus proADAM17) divided by the respective input control. Values were normalised to the respective wt-iRhom2 sample. $n > 4$. **D, E** Levels of surface ADAM17 in cells stably expressing indicated murine iRhom2 constructs (**D**) or human iRhom2 constructs (**E**) were measured by flow cytometry. For quantification, the geometric mean of the specific fluorescence signal was determined and normalised to the respective wt-iRhom2. $n > 4$

overall protein levels. Overall, these findings suggest that the decrease in ADAM17 levels and downregulation of surface ADAM17 seen in the cub deletion and to a lesser extent in the TOC site mutants occur in a FRMD8-independent way. Importantly, the deletion of the TOC site in ndTOC shows a more severe molecular phenotype than the TOC single-point mutations. This is consistent with single point mutations only partially disrupting TOC site functions, whereas a larger deletion has a more severe effect.

The iRhom2 N-terminus differentially regulates ADAM17-mediated shedding

Our findings that cub and TOC mutations decrease levels of matured ADAM17 are in line with recent in vivo and ex vivo results [84, 100]. However, these findings are counterintuitive to the earlier reported elevated ADAM17 shedding activity [14, 39, 40, 42]. To analyse the effect of the N-terminus on ADAM17 activity, we investigated the constitutive shedding of the ADAM17 substrates TGFα, IL1R2 and AREG in HEK293 cells. As reported earlier, we found significantly increased substrate release with additional expression of wt-iRhom2 compared to control cells (Fig. 4A, B) [24, 50]. Surprisingly, despite lower surface ADAM17 levels (Fig. 3D), ADAM17-mediated shedding was not adversely affected in cells with N-terminal deletions nd197, cub and nd349 compared to control cells (Fig. 4A, B). In fact, shedding efficiency in cells with these deletions was generally higher compared to shedding in control cells and comparable to cells expressing wt-iRhom2. The largest deletion nd370 had the lowest ADAM17-mediated shedding but was still comparable to control cells (Fig. 4A, B).

To further investigate the effects of large N-terminal deletions in iRhom2 on ADAM17-mediated shedding in a background free of endogenous iRhoms, we used iRhom1- and iRhom2-deficient mouse embryonic fibroblasts (MEFs) [19]. These cells lack ADAM17 maturation, resulting in an absence of ADAM17-mediated shedding. However, the reintroduction of wt-iRhom2 expression effectively restored ADAM17-mediated shedding (Fig. 4C). Surprisingly, constitutive ADAM17-mediated shedding was also restored for the N-terminal deletions (nd197, cub and nd349), despite barely detectable amounts of ADAM17 present (Fig. S3D). However, the shedding activity restored by the N-terminal deletions was significantly lower compared to cells expressing wt-iRhom2 (Fig. 4C). Interestingly, the largest deletion (nd370), which lacked the third phosphorylation site, showed no restored shedding activity, similar to control cells (Figs. 2G, 4C). Furthermore, we assessed ADAM17-mediated shedding stimulated by the phorbol ester PMA (phorbol 12-myristate 13-acetate). While cells expressing wt-iRhom2 showed a significant increase in shedding, this effect was not observed with iRhom2 deletion mutants (Fig. 4C). This aligns with previous reports indicating that stimulated shedding is primarily driven by phosphorylation at the described phosphorylation sites 1 and 2 [16, 34], which are absent in all deletions (Fig. 2G).

In HEK293 cells, we further investigated the effects of the TOC mutations on AREG shedding. Interestingly, additional expression of human wt-iRhom2 did not significantly increase constitutive AREG shedding (Fig. 4D). This is consistent with our previous findings that overexpression of human iRhom2 promotes shedding to a lesser extent than that of its mouse counterpart [50]. Remarkably, iRhom2 has 96% sequence similarity (92% identity) in human and mouse, except for a large insertion at the beginning of the N-terminus of human iRhom2 isoform 1, which was used in this study (Fig. S3A). The discrepancy in shedding efficiency may be attributed to this dissimilarity.

Importantly, expression of the TOC mutations significantly increased shedding activity (Fig. 4D), consistent with previous observations [12, 63]. Strikingly, we observed even higher shedding efficiency with the complete TOC site deletion ndTOC (Fig. 4D), again showing a more severe molecular phenotype than the single point mutations. Moreover, as expected, iRhom2 with TOC site mutations still promotes PMA-stimulated ADAM17 shedding activity in iRhom1- and iRhom2-deficient MEFs (Fig. 4E). However, the stimulated shedding activity of the TOC site mutants is slightly but significantly reduced compared to wt-iRhom2, which is in line with reduced levels of matured ADAM17 (Figs. 3C, E, 4E).

In summary, our results show that the N-terminus differentially regulates constitutive and stimulated shedding and that the cub deletion loses the ability to promote stimulated ADAM17 activity. Importantly, both larger N-terminal deletions and TOC mutations appear to lead to a reduction in ADAM17 levels with concurrent higher constitutive ADAM17 activity.

N-terminal deletions of iRhom2 accelerate the turn-over of ADAM17

To gain better insight into the molecular phenotypes of N-terminal iRhom2 mutations, we sought to understand the underlying mechanisms. The observed decrease in ADAM17 levels can be attributed to either an impaired maturation process or accelerated turnover leading to increased internalisation of ADAM17 and its lysosomal degradation (Fig. 5A). Previous studies have shown that destabilisation of the iRhom-ADAM17 complex by FRMD8 loss leads to increased lysosomal degradation [55, 77]. However, the effect we observed is FRMD8 independent and has not been studied before. To investigate whether the FRMD8-independent effect of nd197 is due to accelerated degradation, we used the lysosomal inhibitors NH_4Cl and bafilomycin. The

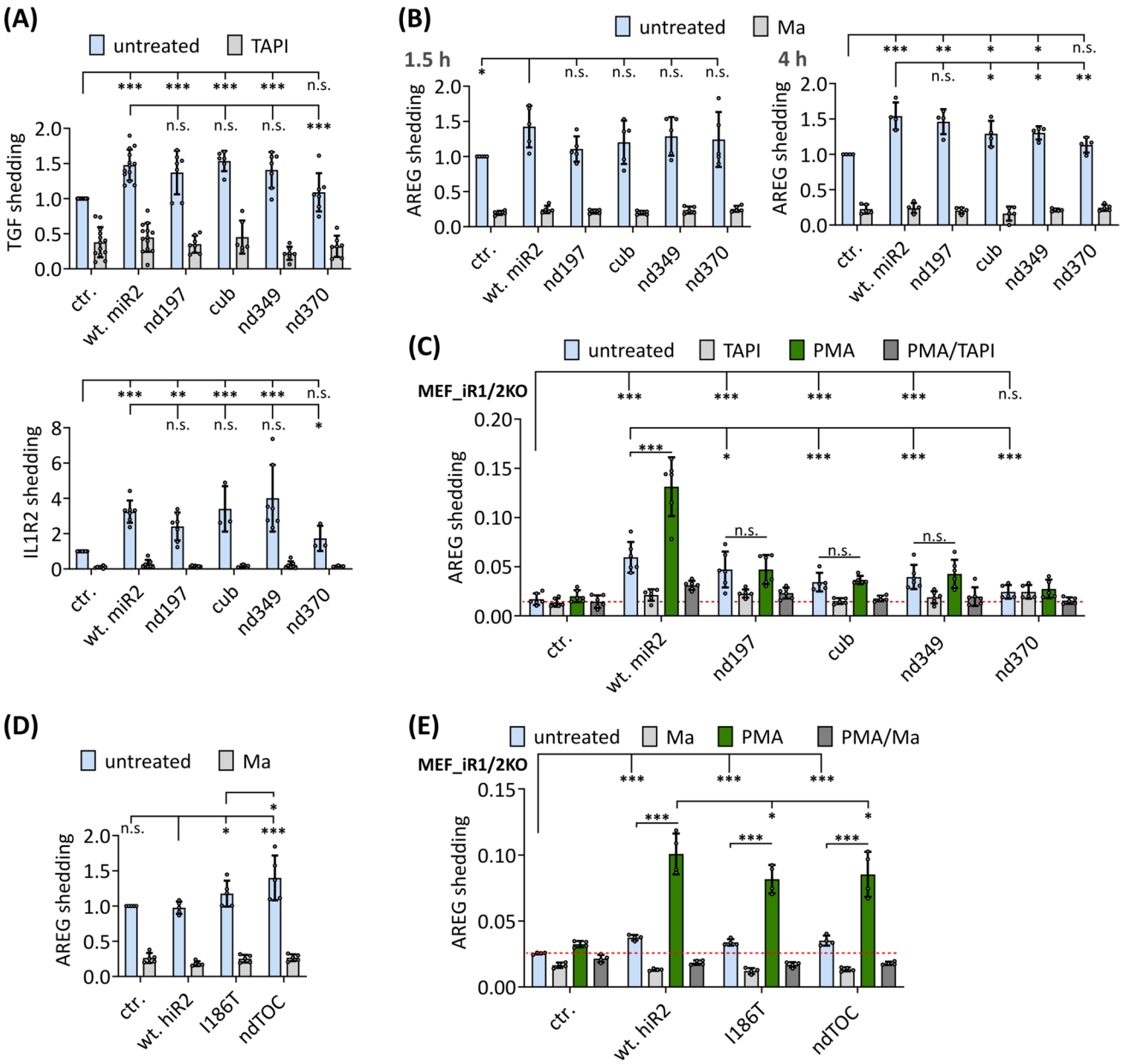


Fig. 4 N-terminal mutations in iRhom2 dysregulate ADAM17-mediated shedding. **A–E** Constitutive ADAM17-mediated shedding activity was assessed by performing an alkaline phosphatase (AP) assay in HEK293 cells (**A,B,D**) and MEFs deficient for iRhom1 and iRhom2 (**C,E**) expressing the indicated iRhom2 constructs. The ADAM17 substrate TGFα, IL1R2 or AREG tagged with AP were used. The metalloprotease inhibitors marimastat (10 µM) or the more ADAM17-specific inhibitor TAPI1 (10 µM) were used as a negative control. Where indicated, ADAM17 activity was additionally stimulated by the phorbol ester PMA (100 nM). $n > 4$

use of these inhibitors for 8 h and 16 h rescued the levels of ADAM17 (Fig. 5B, C). After 16 h, the levels of ADAM17 in HEK293 cells expressing the cub or nd197 deletion reached those of cells expressing wt-iRhom2 (Fig. 5C), indicating a similar maturation efficiency. Therefore, accelerated turnover is likely the cause of the low matured ADAM17 levels when the deletions are expressed. This is consistent with the reduced total levels of ADAM17 in cells expressing the deletions, as maturation is still occurring, which depletes the pool of proADAM17, but ADAM17 is not stable due to accelerated lysosomal degradation.

To further analyse the impact of the iRhom2 N-terminus on the turnover kinetic of ADAM17, we performed a cycloheximide-based pulse-chase experiment (Fig. 5A). We observed a rapid decrease in proADAM17 levels after inhibition of biosynthesis, as the maturation process continued and subsequently proADAM17 levels declined until presumably no iRhom is left in the ER (Fig. 5D). The

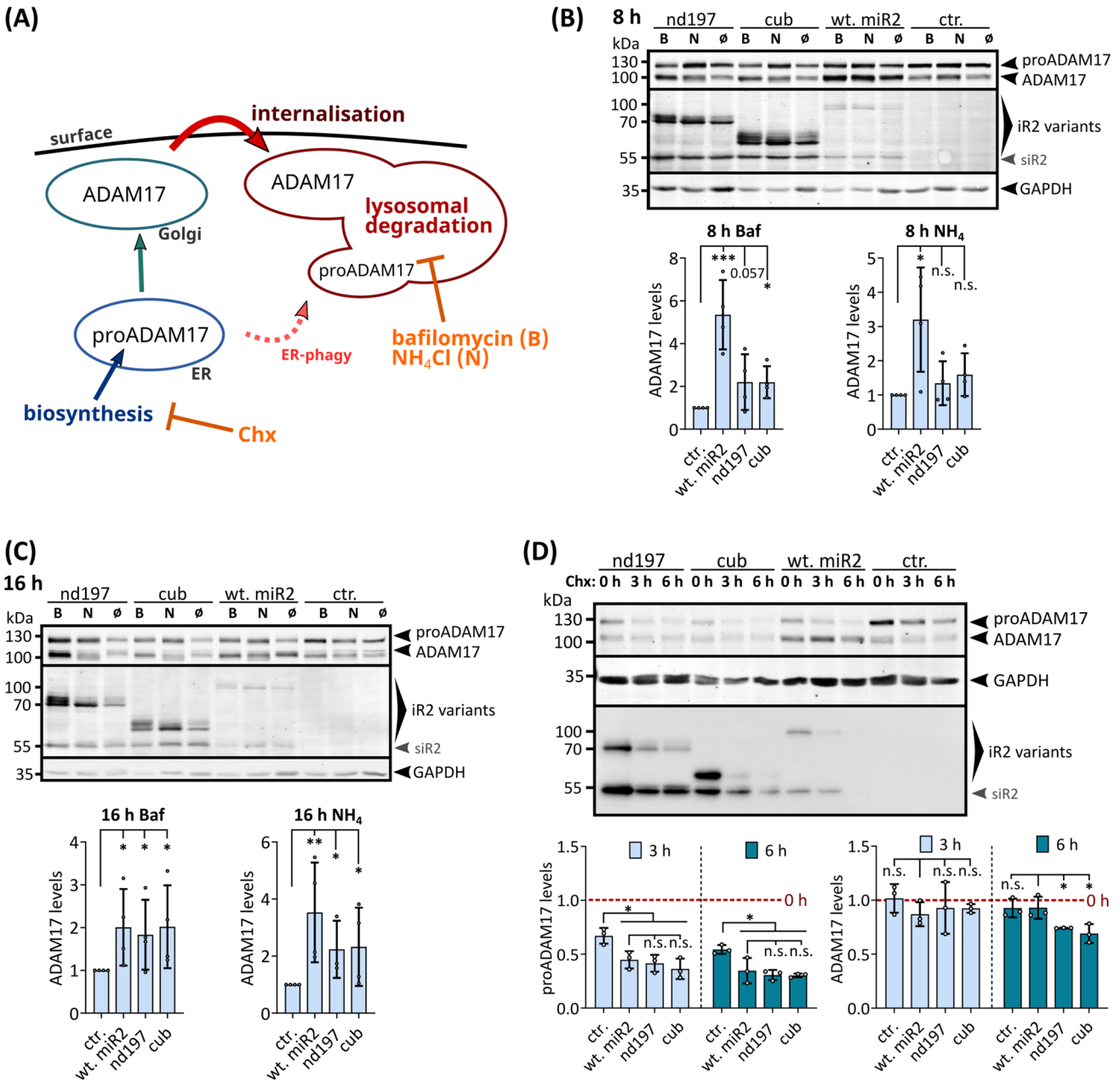
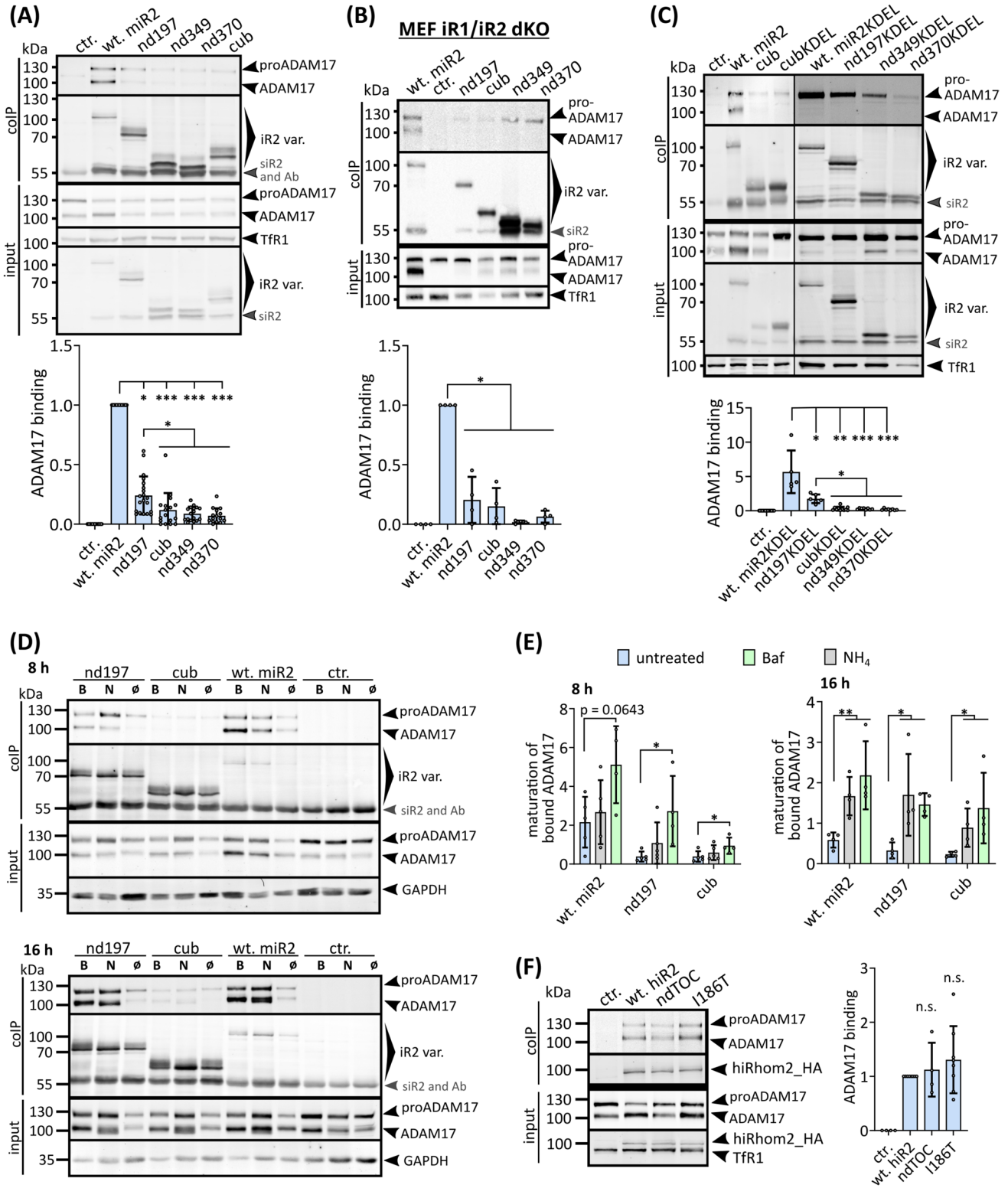


Fig. 5 The N-terminal IDR of iRhom2 regulates protein turn-over kinetics. **A** After biosynthesis in the ER, proADAM17 is transported to the Golgi for maturation with the help of iRhoms. The complex of ADAM17 and iRhom is transported to the cell surface. After internalisation, the complex is degraded in the lysosomes. Like all ER proteins, to a certain extent proADAM17 can be transported directly to the lysosome by ER-phagy. **B, C** To analyse the fate of ADAM17 in cells expressing the nd197 and cub deletion, cells were treated with either NH_4Cl ("N") or bafilomycin ("B") for 8 h (**B**) or 16 h (**C**) to inhibit lysosomal degradation. Levels of ADAM17 were assessed by densitometric measurements and calculation of the ratio between ADAM17 and the loading control GAPDH, which is independent of lysosomal degradation. ($n=4$) **D** To assess the turn-over rate of ADAM17 a cycloheximide-based (Chx) pulse-chase experiment was performed. Reduction of ADAM17 levels was assessed by densitometric measurements and normalisation to 0 h Chx treatment (set to 1). ($n=3$)

presence of wt-iRhom2 facilitated this effect, significantly enhancing the reduction due to increased ADAM17 transport to the Golgi and subsequent maturation. We found that nd197 and cub deletions had the same effect (Fig. 5D), indicating that the maturation process remained unaffected by the N-terminal deletions.

Furthermore, the levels of ADAM17 decreased more rapidly in cells expressing the deletion than in control cells



or cells expressing wt-iRhom2 (Fig. 5D) indicating accelerated degradation of ADAM17 in the presence of N-terminal deletions.

For comparison, we next studied the influence of TOC mutations on ADAM17 stability. 8 h of bafilomycin-mediated lysosomal inhibition rescued the levels of ADAM17 in cells expressing the TOC mutant to the same level as cells with wt-human iRhoms (Figure S3E). This suggests that the same amount of ADAM17 is generated in cells expressing TOC mutants or wt-human

◂**Fig. 6** The N-terminus of iRhom2 regulates ADAM17 interaction. To analyse the interaction between ADAM17 and the indicated iRhom2 variants, coIPs were performed using the iRhom variants (with HA tag) as bait. Immunoblotting and subsequent densitometric measurements were used to quantitatively analyse iRhom2-ADAM17 binding (ratio of co-precipitated ADAM17 and precipitated iRhom2) and normalised to wt-iRhom2. **A** HEK293 stably expressing indicated iRhom2 variants or GFP (ctr.) were used ($n > 17$). **B** MEFs from mice deficient for iRhom1 and iRhom2 stably expressing indicated iRhom2 variants or GFP (ctr.) were used ($n = 4$). **C** HEK293 expressing indicated iRhom2 variants or GFP (ctr.) fused to the ER-retention motif KDEL were used ($n > 5$). **D, E** To analyse the fate of ADAM17 specifically in the iRhom2-ADAM17 complex containing either the nd197 deletion, cub deletion or wt-iRhom2, cells were treated with either 40 mM NH_4Cl (N) or 500 nM bafilomycin (B) for 8 h or 16 h to inhibit lysosomal degradation. Maturation levels of bound ADAM17 was assessed by densitometric measurements and calculation of the ratio between ADAM17 and proADAM17. The quantitative analysis of ADAM17 binding can be found in Fig. S4C. ($n = 4$). **F** HEK293 stably expressing indicated human iRhom2 variants or GFP (ctr.) were used for coIP experiments as described above. ($n > 4$)

iRhom2. Lysosomal degradation of ADAM17 is slightly higher in cells with TOC mutations than in cells expressing wt-iRhom2, resulting in slightly lower levels of total matured ADAM17 and less ADAM17 on the cell surface, as described above (Fig. 3C, E). However, this slightly accelerated degradation does not seem to be strong enough to detect significant differences with the cycloheximide-based pulse-chase experiments (Figure S3F).

Taken together, these results demonstrate the regulatory role of the N-terminus in controlling the stability and turnover kinetics of ADAM17, but not proADAM17. In addition, the effects of larger deletions are more severe compared to mutations or deletions at the TOC site, suggesting that the stability of ADAM17 is only slightly affected by the TOC site, but is more dependent on the interplay of other sites in the iRhom2 N-terminus. As there is no difference between nd197 and cub, this mechanism appears to be FRMD8 independent.

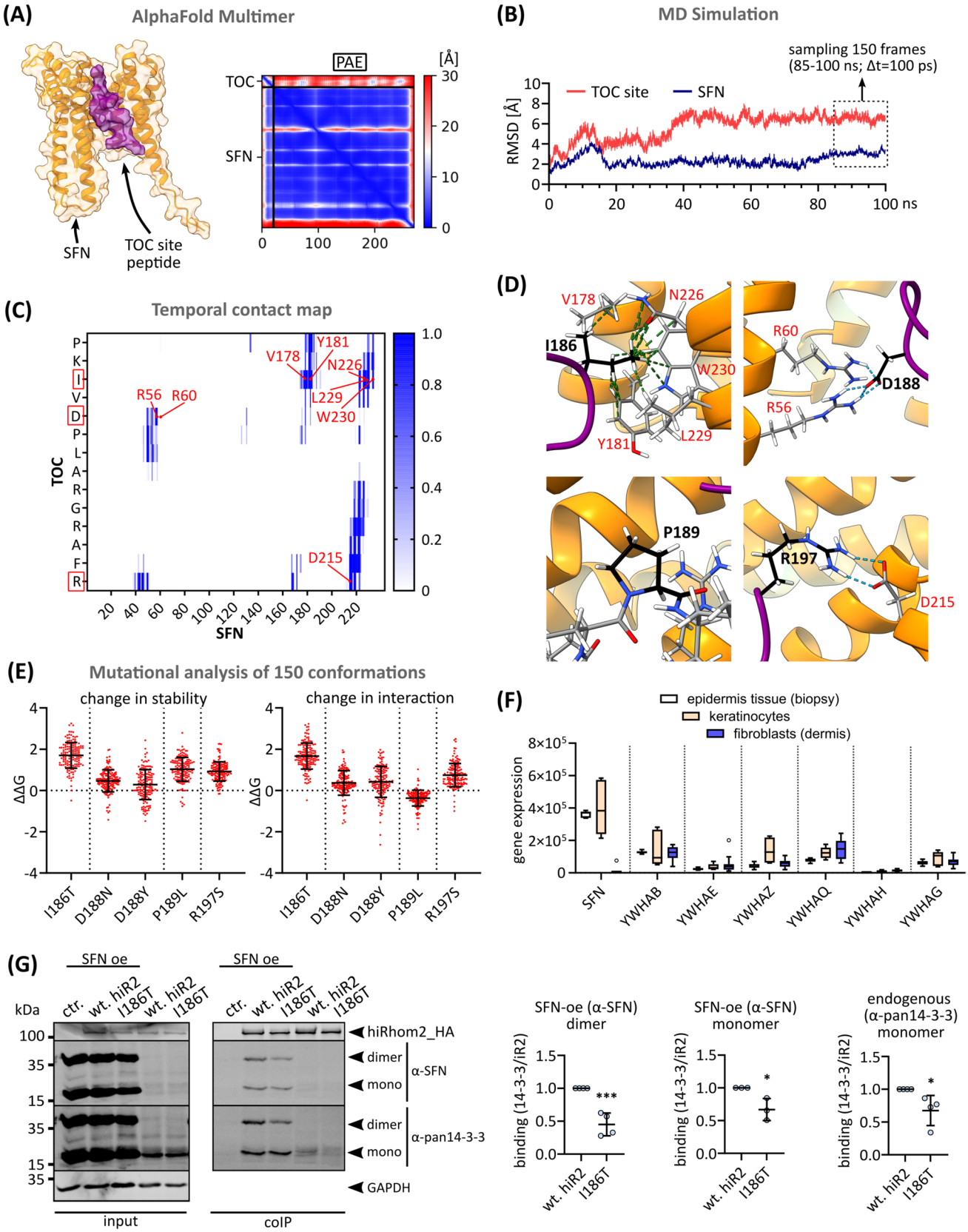
The iRhom2 N-terminal IDR is a key determinant for regulating ADAM17 binding

The interaction between iRhom and ADAM17 is a crucial requirement for their stability. Although the transmembrane regions and extracellular domains are known determinants of the binding between iRhom and ADAM17 [16, 24, 34, 50, 58], we nevertheless wondered whether the N-terminus could play a role in this interaction. By co-immunoprecipitation, we analysed the binding between ADAM17 and iRhom2. In both HEK293 cells and iRhom1- and iRhom2-deficient MEFs, we observed a significant decrease in binding between ADAM17 and all deletions tested (nd197, cub, nd349 and nd370) compared to wt-iRhom2 (Fig. 6A,B). However, the overall decrease in cellular ADAM17 levels could distort the results. To address this issue, we engineered iRhom2 variants fused to the ER retention sequence KDEL, which inhibits ADAM17 transport, maturation, and subsequent accelerated turnover of the iRhom2-ADAM17 complex (Fig. S4A) [24]. In fact, even in this setting, we found a significant reduction in ADAM17 binding for iRhom2 deletions compared to wt-iRhom2 (Fig. 6C; Fig. S4B). Interestingly, we detected an additional significant reduction in ADAM17 binding for deletions larger than nd197, indicating multiple regions in the N-terminus that regulate ADAM17 binding (Fig. 6A, C). This observation is consistent with co-immunoprecipitation experiments using lysosomal inhibitors, where inhibition of lysosomal degradation significantly increased the observable intact iRhom2-ADAM17 complex with nd197, but not with cub deletion (Fig. S4C). Under lysosomal inhibition, the precipitated complexes with nd197 and cub showed increased amounts of ADAM17 indicating more rapid degradation when in complex with these deletions (Fig. 6D, E). Importantly, we did not observe a reduction in the binding efficiency of the TOC site mutants (Fig. 6F).

In summary, our results clearly demonstrate the crucial role of the N-terminus in the binding affinity between iRhom2 and ADAM17, which in turn influences the cohesion and stability of the iRhom2-ADAM17 complex. Remarkably, there appear to be two parallel mechanisms regulating the ADAM17 interaction via the N-terminus: a clearly FRMD8-independent mechanism and a potential FRMD8-dependent mechanism. Importantly, this ADAM17 interaction function is lost in the larger cub deletion but not when only the TOC site is disrupted (Fig. 7).

The TOC site represents a phosphorylation-independent 14-3-3 binding site

Using AlphaFold Multimer complex modelling, we screened the TOC site for interaction with putative iRhom2 binding partners that we and others had previously reported [16, 24, 34]. Thereby we identified 14-3-3σ/stratifin (SFN) as a potential interactor for the TOC site (Fig. 7A). To analyse the dynamic nature of the TOC-site-SFN complex, we performed molecular dynamics simulations and sampled 150 conformations within the RMSD (root-mean-square deviation) equilibrium (Fig. 7B). A contact map based on this conformational assembly revealed the interacting residues between the TOC site and SFN (Fig. 7C, D). Specifically, I186 interacts with a hydrophobic cleft in SFN, while D188 and R197 form salt bridges with SFN residues (Fig. 7D). P189 shows no direct interaction but appears to maintain a local structure important for overall binding with SFN (Fig. 7D, E). Strikingly, D188 forms a salt bridge with R56 and R60 of SFN, which are part of the region that normally facilitates interaction with phosphorylated serine residues of


(A)
AlphaFold Multimer
SFN
TOC site peptide
PAE
TOC
SFN
[Å]
30
20
10
0
0
100
200
(B)
MD Simulation
sampling 150 frames
(85-100 ns; Δt=100 ps)
TOC site
SFN
RMSD [Å]
10
8
6
4
2
0
0
20
40
60
80
100 ns
(C)
Temporal contact map
TOC
P
K
I
V
D
P
L
A
R
G
R
A
F
R
Y181
V178
N226
R56
R60
L229
W230
D215
1.0
0.8
0.6
0.4
0.2
0
20
40
60
80
100
120
140
160
180
200
220
SFN
(D)
V178
N226
I186
W230
Y181
L229
R60
D188
R56
P189
R197
D215
(E)
Mutational analysis of 150 conformations
change in stability
change in interaction
ΔΔG
4
2
0
-2
-4
I186T
D188N
D188Y
P189L
R197S
(F)
epidermis tissue (biopsy)
keratinocytes
fibroblasts (dermis)
gene expression
8×10^5
6×10^5
4×10^5
2×10^5
0
SFN
YWHAB
YWHAE
YWHAZ
YWHAQ
YWHAH
YWHAG
(G)
SFN oe
SFN oe
kDa
ctr.
wt. hiR2
I186T
wt. hiR2
I186T
100
35
15
35
15
35
hiRhom2_HA
dimer
mono
α-SFN
dimer
mono
α-pan14-3-3
GAPDH
input
coIP
SFN-oe (α-SFN) dimer
SFN-oe (α-SFN) monomer
endogenous (α-pan14-3-3) monomer
binding (14-3-3/iR2)
1.5
1.0
0.5
0.0
***
*
*
wt. hiR2
I186T

◂**Fig. 7** The TOC site binds 14-3-3 proteins in a phosphorylation-independent manner. **A** The complex consisting of the TOC site peptide (P184 to R197) and 14-3-3σ/stratifin (SFN) was modelled with AlphaFold Multimer. The highest-ranked model and its PAE score are shown. **B** The highest-ranked AlphaFold model of the SFN-TOC site complex was used for molecular dynamics simulation. RMSD changes during the simulation run are shown. 150 frames/conformations between 85 and 100 ns ($\Delta t = 100$ ps) were extracted for subsequent analysis. **C** Combined Cα contact map of all 150 sampled conformations indicates the frequency of contacts between SFN and TOC site over time. Identified interactions between positions of TOC mutants and residues in SFN are labelled. **D** Visualisation of interactions between pathologically relevant residues in the wt TOC site with residues of SFN: cartoon representation of conformation at 92 ns of MD simulation. I186 interacts with a hydrophobic cleft in SFN. D188 and R197 form salt bridges. P189 shows no interaction. **E** Changes in overall complex stability and binding energies were calculated for the pathological TOC mutations for all 150 conformations: $\Delta\Delta G < 0$ indicates improved stability/binding; $\Delta\Delta G > 0$ indicates decreased stability/binding. **F** Gene expression levels of 14-3-3 proteins in epidermis and primary keratinocytes and primary fibroblasts. **G** To analyse the interaction between 14-3-3 proteins and the indicated iRhom2 variants, coIPs were performed using the indicated iRhom variants (with HA tag) as bait. SFN was additionally overexpressed (oe) in the indicated samples. Immunoblotting and subsequent densitometric measurements were used to quantitatively analyse iRhom2-14-3-3 protein binding (ratio of co-precipitated 14-3-3 protein and precipitated iRhom2) and normalised to wt iRhom2. Notably, the dimeric form of oe SFN appears to be somewhat resistant to SDS

14-3-3 clients. Thus, D188 appears to mimic a phosphoserine residue, facilitating a phosphorylation-independent mode of 14-3-3 binding. The consequences of the pathological TOC mutations on the complex stability and interaction energies were assessed and, as expected, showed a profound effect on the complex integrity (Fig. 7E). Based on these findings, we investigated whether overexpressed SFN, which is predominantly expressed in skin and undetectable at endogenous levels in HEK293 cells (Fig. 7F, G), shows altered interaction efficiency between wt iRhom2 and the I186T TOC mutant. Indeed, using coIPs, we found that the I186T TOC mutant showed reduced interaction with SFN compared to wt iRhom2 (Fig. 7G). These data are in line with our in silico analysis and confirm the role of I186 within TOC for efficient SFN binding. Using a pan-14-3-3 antibody, we also found that other 14-3-3 isoforms expressed endogenously interact with the TOC site (Fig. 7G).

Overall, the TOC site serves as a phosphorylation-independent 14-3-3 binding site and this interaction is disrupted by pathological TOC mutations.

Discussion

The iRhom2-ADAM17 sheddase complex is vital for both inflammatory signals (including TNFα release) and EGFR signalling (via growth factor release such as AREG and TGFα). iRhom2 is a key regulator for ADAM17's trafficking, maturation, activity, and stability. Understanding its regulation is crucial for the molecular biology of ADAM17-associated diseases and, consequently, for potential therapies targeting these pathologies. These include chronic inflammation and cancer pathologies, such as the autosomal dominant hereditary disorder tylosis with oesophageal carcinoma (TOC) [12, 25]. TOC is caused by mutations in the cytosolic N-terminus of iRhom2, resulting in increased ADAM17 activity, elevated growth factor release and increased EGFR signalling [12, 14, 39, 40, 42, 66]. Mice with the cub (curly-bare) deletion exhibit a similar phenotype to mice with TOC mutations, and both phenotypes can be rescued by knocking out amphiregulin [40, 42]. This suggests a shared molecular mechanism between the large cub deletion and TOC single-point mutations. However, studies on the cub deletion have yielded conflicting findings regarding whether it has a positive or negative effect on ADAM17 shedding activity [34, 41, 63, 84, 100]. In contrast, TOC mutations in iRhom2 increase ADAM17-mediated shedding [12, 14, 41], which is consistent with our results. In addition to TOC single point mutations, we used a complete deletion of the TOC site, resulting in an even more pronounced effect.

We identified the TOC site as a phosphorylation-independent 14-3-3 protein binding site that appears to have a restrictive effect on constitutive ADAM17 activity, which is disrupted by pathological TOC mutations (Fig. 8). 14-3-3 proteins, as phosphoserine and phosphothreonine binding proteins, regulate most cellular processes. With widespread expression in tissues, they serve as universal scaffolds, influencing the structure and function of diverse protein targets in key cellular signalling pathways (Obsilova et al. 2022). Although the majority of reported 14-3-3 binding motifs involve phosphorylation, there are a few non-canonical examples. In particular, the L**D**LA box in the exoenzyme S of *Pseudomonas aeruginosa* and the WL**D**LE motif in the artificial peptide R18 show high affinity to 14-3-3 proteins (Obsilova et al. 2022). These motifs consistently feature an aspartate residue surrounded by hydrophobic residues, which bears a striking resemblance to the IV**D**PL motif found within the TOC site. Our finding is also consistent with previous results that the TOC site may also facilitate binding to keratin [66]. 14-3-3 proteins are known to interact with keratins [53] and may therefore act as an adapter between iRhom and keratins.

In contrast, the larger cub deletion, which includes the entire TOC site, has more molecular consequences (Fig. 8): (1) The loss of stimulated ADAM17 activity is consistent with the loss of N-terminal phosphorylation sites. (2) Large deletions of the N-terminus reduce the efficiency of iRhom-ADAM17 interaction and accelerate ADAM17 degradation, resulting in reduced levels of ADAM17 and reduced ADAM17 surface localisation.

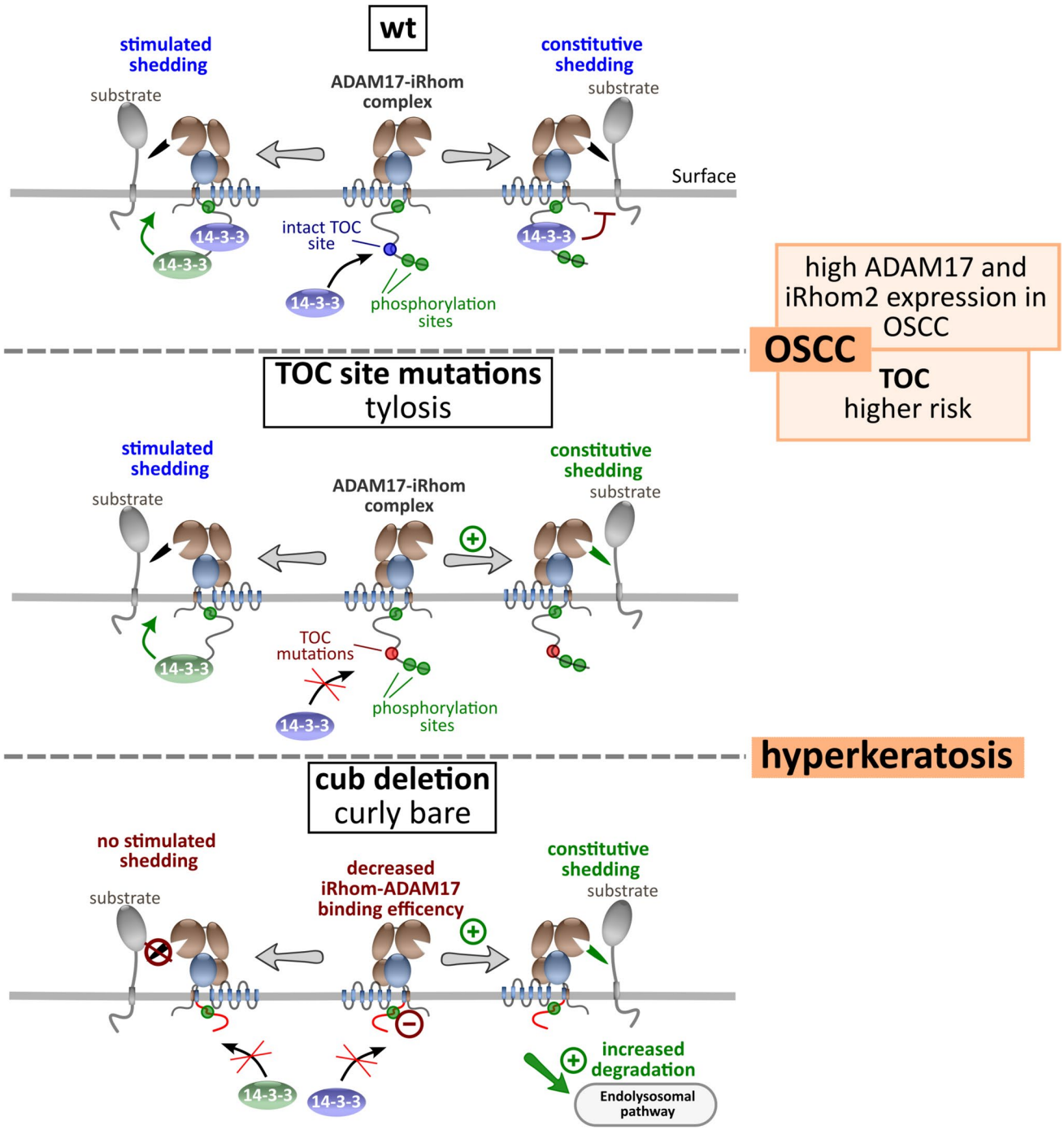


Fig. 8 The iRhom2 N-terminal IDR regulates ADAM17 binding and shedding activity. Wt iRhom2 plays a critical role in regulating the transport, maturation, constitutive and simulated shedding activity of ADAM17, ensuring proper control of downstream signalling pathways such as EGFR activation. Conversely, disruption of the TOC site in the N-terminal IDR of iRhom2 results in loss of phosphorylation-independent 14-3-3 binding and appears to result in dysregulated higher constitutive shedding activity. Hyperkeratosis and increased risk of OSCC, which also shows higher iRhom2 and ADAM17 expression, are known consequences of TOC mutations. In the case of the cub deletion, not only is the TOC site disrupted, but efficient binding to ADAM17 is also impaired, accelerating ADAM17 turnover and lysosomal degradation. In addition, the cub deletion loses its ability to promote stimulated ADAM17 shedding activity. It is likely that the lack of phosphorylation-dependent 14-3-3 binding plays a key role in this process

Previously identified phosphorylation-dependent 14-3-3 binding to the iRhom N-terminus appears necessary for stimulated shedding [16, 34] (Fig. 8). In contrast, constitutive shedding may be attenuated by efficient 14-3-3 binding to the TOC site, which would be consistent with previously reported ADAM17 hyperactivation when the TOC site is mutated or missing [12, 41, 42, 63].

Interestingly, the largest deletion we used, nd370, which is also missing a third key phosphorylation site and putative 14-3-3 binding site (Fig. 2G) [16, 34], additionally shows abolished constitutive shedding. Taken together, these suggest that there are distinct signalling pathways that differentially regulate 14-3-3 binding and, in turn, constitutive and stimulated ADAM17 activity. More studies are needed to dissect these complex mechanisms.

Notably, recent studies have also highlighted the critical role of the KRAS-ERK1/2 pathway in the shedding activity of the iRhom2-ADAM17 complex [16, 34, 98]. KRAS-G12 mutants in tumour cells harbouring iRhom2 with TOC mutations further enhance constitutive ADAM17-mediated shedding [98]. Interestingly, an ERK2 binding site was recently identified within the N-terminus upstream of phosphorylation sites 1 and 2 (Fig. 2G) [95]. Since this ERK2 interaction site is not present in cub, it appears to be more relevant for stimulated shedding rather than constitutive shedding.

The N-terminus of iRhoms emerges as a critical determinant for the stability and activity of the iRhom-ADAM17 complex. Recent findings highlight the significance of FRMD8-binding in regulating iRhom stability and, consequently, ADAM17 stability and functions [55, 77]. While the loss of FRMD8 binding may contribute to the molecular consequences observed in cub deletions, our observations demonstrate similar effects on ADAM17 stability in the nd197 deletion, which retains the ability to bind FRMD8. This suggests that the N-terminus exerts a stabilising effect on the iRhom-ADAM17 complex, largely independent of FRMD8: When these parts of the iRhom2 N-terminus, which are not involved in FRMD8 binding, are deleted, accelerated turnover still occurs. Notably, TOC mutants also show an effect on the stability of ADAM17, but to a lesser extent.

Our study reveals that not only the transmembrane helix 1 and the IRHD, as previously described [24, 50, 58, 106], but also the iRhom2 N-terminus, contributes to ADAM17 binding. Through our ER-trapping approach, we have demonstrated that the reduced binding of ADAM17 is not attributable to decreased ADAM17 levels. Notably, the anterior half of the N-terminus (nd197) emerges as particularly crucial for efficient ADAM17 interaction. However, larger deletions like the cub deletion (Δ268) result in an additional significant reduction in binding efficiency, potentially mediated by FRMD8.

We postulate that while the binding affinity to ADAM17 is significantly reduced, iRhom2 N-terminal deletions such as cub retain the ability to bind proADAM17 in the ER, facilitating efficient transport through the secretory pathway and normal maturation of ADAM17. During maturation, the proteolytic removal of the ADAM17 prodomain may further decrease binding affinity, as our recent study identified the prodomain as an additional binding determinant between the ADAM17 ectodomain and the IRHD [50]. The reduced cohesion of the iRhom2-ADAM17 complex on the cell surface appears to induce instability and accelerated turnover, culminating in lysosomal degradation (Fig. 8).

In our study, we focused on the molecular functions of the iRhom2 N-terminus to unravel the intricate regulatory system of the iRhom2-ADAM17 complex. Our study did not explore the integration of these mechanisms into a more complex in vivo system. Importantly, the recent study by Rabinowitsch et al. [84] found similar results in terms of ADAM17 levels and shedding activity in vivo using different mouse lines, including cub/cub mice and TOC/TOC mice. They also found reduced ADAM17 levels in different tissues when the cub mutation is present, as we observed in our in vitro experiments. Our study complements this finding by demonstrating with our lysosomal inhibition and cycloheximide-based pulse-chase experiments that the lower ADAM17 levels are indeed the result of accelerated turnover and not reduced maturation. By using additional shorter deletions of the N-terminal IDR of iRhom2, we also provide evidence that this effect is independent of FRMD8 binding. Since we found that the cub deletion and an even shorter deletion of the N-terminal IDR of iRhom2 reduced binding to ADAM17, we can speculate that this reduces ADAM17 stability and leads to its accelerated lysosomal degradation.

The results of Rabinowitsch et al. [84] and our results are also consistent in terms of the loss of stimulable shedding activity when only iRhom2 with the cub deletion is present. Furthermore, at the cellular level, Rabinowitsch et al. [84] and we observed a reduction in constitutive shedding when only iRhom2 with the cub deletion is present. Again, we observed this with an even shorter deletion. This contrasts with previous reports of higher ADAM17 shedding activity with cub [40, 41]. One difference may be the genotype used, as Hosur et al. [40] used mice with endogenous iRhom1 still present, whereas Rabinowitsch et al. [84] analysed the effect of the cub deletion by using iRhom1 knock-out mice. In general, the gene expression and protein levels of iRhom1 and iRhom2 in these different wt and mutant mice, as well as in the different cell lines used in these in vivo and ex vivo studies, need to be determined in future research as this may be important to further understand these contrasting results. Interestingly, cub deletion in our study only slightly reduces ADAM17 activity compared to wt iRhom2 in the presence of endogenous iRhom, but also results in a

profound reduction of ADAM17 on the cell surface. Taking this into account, the shedding activity per ADAM17 molecule appears to be upregulated, while the overall shedding activity at the cellular level appears to be reduced.

Importantly, ADAM17 activity at the cellular level in vivo is dependent on cell type-specific endogenous protein levels of iRhom1, iRhom2 and ADAM17, which will also influence the manifestations of pathological changes in the iRhom-ADAM17 axis [84]. Here it is also important to consider that ADAM17 substrate specificity appears to be differentially regulated by iRhom1 and iRhom2 [65, 106]. In addition, iRhom functions independent of the ADAM17 pathway may also be involved in the manifestation of TOC and cub pathologies. For example, the N-terminus of iRhom can be cleaved and translocated into the nucleus where it exerts incompletely understood effects on gene expression [23, 122]. It is also critical to recognise that altered ADAM17 activity can also initiate feedback loops that further modulate its own activity, including the induction of ADAM17 activity by activation of the EGF receptor pathway [34, 54, 98] and induction of gene expression of ADAM17, iRhoms and other regulators through various pathways including TNFα signalling [6, 8, 33, 54]. In addition, exogenous stimuli and cell stimulation, for example by LPS, also affect ADAM17 activity and gene expression of iRhom2, ADAM17 and its substrates [7, 24, 61, 67].

As the TOC mutations affect iRhom2, it is important to note that high iRhom2 expression is often predominantly associated with immune cells and inflammatory conditions. This role of iRhom2 becomes apparent when considering that mice lacking iRhom2 have a seemingly healthy phenotype but show impaired immune responses [2, 19, 46]. However, the high level of iRhom2 gene expression we observed in keratinocytes highlights the important role of iRhom2 in skin homeostasis. This would be consistent with the TOC skin hyperkeratosis phenotype and, in contrast, the reduced thickness of stress calluses in iRhom2 KO mice described previously (Fig. 8) [12, 14, 63, 66]. Notably, in patients with TOC mutations, tylosis manifests between the ages of 7 and puberty, while cancer develops much later in life [28], hinting at a cumulative effect over time. This is in line with our finding that disruption of the TOC site leads to a gradual effect on iRhom2-ADAM17 complex functions: The larger deletion of the TOC site has a stronger effect on ADAM17 activity than single point mutations.

Furthermore, we found a significant increase in iRhom2 and ADAM17 gene expression in oesophageal squamous cell carcinoma (OSCC) compared to healthy oesophageal squamous tissue. This indicates that the iRhom2-ADAM17 complex is a potential tumour marker for OSCC, which seems to be in line with the fact that patients with TOC mutations, which increase ADAM17 activity, have a higher risk of developing OSCC (Fig. 8).

Overall, our results shed new light on the regulation of the iRhom2-ADAM17 complex by the cytosolic N-terminal IDR of iRhom2. The intrinsically disordered nature of the N-terminus makes it an extensive hub for protein binding and regulation. The molecular functions highlighted in our study warrant further analysis and could potentially serve as viable targets for modulating ADAM17 activity. They could offer promising avenues for combating ADAM17-associated pathologies such as cancer or chronic inflammation.

Methods

Bioinformatics

Multiple sequence alignments were generated by utilising Clustal Omega [99]. Secondary structure prediction and analysis of intrinsically disordered regions were done with IUPred3 [29, 70], NetSurfP-2.0 [52] and ANCHOR2 [21, 69, 70]. The following sequences were used (UniProtKB entries): Q6PJF5 (human iRhom2) and Q80WQ6 (murine iRhom2). Nuclear localisation sequence analysis was performed with NLStraddamus [74].

To identify conserved sequence regions, the tool CONYAR (Conserved You Are) was employed to perform high-throughput comparison of as many sequences of a target protein as possible [50].

Structural modelling and molecular dynamics simulations

Ab initio structure prediction of the cytosolic iRhom2 N-terminus was done with AlphaFold2 and AlphaFold Multimer [49] utilising ColabFold [71]. Structural modelling using the deep learning algorithm AlphaFold2 was done without homology templates. MMseq2 was used as the multiple sequence alignment. Structural modelling was performed in 12 iterations. ChimeraX was used to visualise the structures [81].

Molecular dynamics simulation was used to analyse the dynamics of the SFN-TOC-site complex over time. The highest-ranked AlphaFold model of the complex was used. The system was immersed in TIP3P water in a cubic box with 1.0 nm padding and neutralised with 150 NaCl. The MD simulation was performed using GROMACS2020.6 [82] with the AMBER99SB-ILDN force field [60]. The system was first energy minimised. Equilibration MD simulations were performed with periodic boundary conditions. The temperature was equilibrated using an NVT ensemble for 1 ns followed by an NPT ensemble for 1 ns to equilibrate the pressure using the v-rescale temperature and Parrinello – Rahman pressure coupling method during production. Finally, the production MD simulations were

performed for 100 ns (300 K and 1 atm). Between 85 and 100 ns, which was within RMSD equilibrium, 150 conformations/frames were sampled (Δt = 100 ps). Biopython [20] was used to calculate the distances between Cα within this conformational compilation of each frame and to generate a temporal contact map (cutoff < 12 Å) with the frequency of contacts within the sampled 15 ns. FoldX (v5) PSSM and Position Scan [111] were used to analyse the influence of single point mutations in the sampled conformations on binding and overall stability, respectively.

In silico gene expression analysis

We accessed Affymetrix Human Genome U133 Plus 2.0 Array platform data from public repositories, curated by the GENEVESTIGATOR platform (Immunai, USA) [44]. The GENEVESTIGATOR software was utilised for gene expression meta-analysis of indicated genes in various tissues, biopsies, and primary cells (assessed on 20 May 2023). To analyse gene expression patterns under physiological conditions, only samples from healthy and untreated tissues were included. Similarly, for assessing baseline gene expression in cancerous tissue, only untreated samples were considered.

List of used experiment IDs for indicated tissue and primary cells: a) murine heart: MM-00170 [73], MM-00253 [22], MM-00257 [124], MM-00262 [3], MM-00300 [85], MM-00322, [107], MM-00330 [57], MM-00368 [9], MM-00384 [118], MM-00476 [1], MM-00485 [78], MM-00492 [115], MM-00497 [97], MM-00507 [97], MM-00561 [86], MM-00834 [108], MM-00841 [68], MM-01538 [31], MM-01642 [62], MM-01875 [62]; b) murine primary fibroblast (dermis): MM-00159 (Vallender et al. 2006), MM-00180 (Vallender et al. 2006), MM-00627 [32], MM-00724 [32]; c) murine primary keratinocytes: MM-01215 [4]; d) healthy human epidermis tissue (biopsy): HS-02924 [30]; e) human primary keratinocytes (untreated): HS-02625 [121], HS-02787 [15], HS-02490 [105], HS-00220 [90]; f) human primary keratinocytes (treated with TNFα, IFNα, IFNγ or IL4; 24 h): HS-02490 [105]; g) human primary keratinocytes (treated with 10 ng/ml I IFNγ; 96 h): HS-02625 [121]; h) human primary fibroblasts (untreated): HS-00393, HS-00481 [18], HS-00805 [112], HS-00928 [117], HS-00963, HS-00989 [104], HS-01109 [113], HS-01279 [64], HS-01311 [36], HS-01326 [114], HS-02421 [102],i) primary artery smooth muscle cells (heart): HS-00478 [96]; j) primary bronchial smooth muscle cells: HS-00039 [13]; k) healthy oesophagus squamous tissue (biopsy): HS-01298 [116], HS-00217, HS-00017 [88], HS-01525 [93]; squamous cell carcinoma (grade G1): HS-01298 [116]; oesophagus adenocarcinoma: HS-00002; HS-01298 [116]; Barrett´s oesophagus (pre-malignant): HS-01298 [116]; primary macrophages: HS-01265; primary granulocytes: HS-00250; primary leukocytes: HS-00261; primary monocytes: HS-01403.

Cloning

The cloning procedures were performed as previously described [24]: NEBuilder HiFi DNA Assembly Master Mix (NEB, E2621L) was utilised to produce different plasmids with the desired inserts according to the manufacturer's instructions. All iRhom constructs were cloned into the pMOWS backbone [24, 51]. Site-directed mutagenesis was performed using overlapping PCR [37].

Cell culture

All cells were cultured in a humidified incubator at 37 °C, 5% CO_2 in DMEM10% (unless otherwise indicated). DMEM10% consists of DMEM high-glucose (Sigma-Aldrich) supplemented with 10% foetal calf serum (Pan-Biotech), 100 mg/l streptomycin (Sigma-Aldrich) and 60 mg/l penicillin (Sigma-Aldrich). Production of stable cell lines was done as described before [24]. MEFs double deficient for iRhom1 and iRhom2 were obtained from indicated mouse lines as described before [19, 24]. HEK293 cells were purchased from the German Collection of Microorganisms and Cell Cultures (GmbH DSMZ- No. ACC 305). Normal human epidermal keratinocytes and human dermal fibroblasts were isolated from human skin samples as described before [94]. Primary keratinocytes were cultivated in Dermalife K—Life Line (Cell Systems LL-0007). Primary fibroblasts were cultivated in DMEM10%.

Quantitative PCR (RT-qPCR)

mRNA expression levels were measured by quantitative PCR and normalised to the mRNA expression levels of the selected reference genes. Cytochrome c1 (CYC1) and ribosomal protein L13a (RPL13A) were chosen as the most stable reference genes based on the results from the CFX Maestro Software 1.1 (Bio-Rad). RNA was extracted using RNeasy Kit (Qiagen) and quantified photometrically (NanoDrop, Peqlab, Erlangen, Germany). For reverse transcription, the PrimeScriptTM RT Reagent Kit (Takara Bio Europe) was used, according to the manufacturer's protocol. PCR reactions were performed in duplicates of 10 µl volume comprising 1 µl of cDNA template, 5 µl iTaq Universal SYBR Green Supermix (Bio-Rad), 3 µl H_2O and 0.5 µl forward and reverse primer. The following primers were used with the primer annealing time given in brackets: CYC1 (forward: AGC TAT CCG TGG TCT CAC C, reverse: CCG CAT GAA CAT CTC CCC ATC; 59 °C), iRhom1 (RHBDF1) (forward: GAC AGC CCA CAT CTC TTC AC, reverse: TCC TTG CTC ACT CCA AAC CA; 56

°C), iRhom2 (RHBDF2) (forward: CGA TTG ACC TGA TCC ACC, reverse: CAA AGT CTC CGA GCA GTC C; 58 °C) and RPL13A (forward: GCC CTA CGA CAA GAA AAG CG, reverse: TAC TTC CAG CCA ACC TCG TGA; 60 °C). All RT-qPCR reactions were performed on a CFX Connect Real-Time PCR Detection System (Bio-Rad) using the following protocol: 40 cycles of 10 s denaturation at 95 °C, followed by 10 s annealing at the corresponding temperatures and 15 s amplification at 72 °C. PCR efficiency was calculated from the uncorrected RFU values using LinRegPCR version 2020.0 [89]. CFX Maestro Software 1.1 (Bio-Rad) was used for relative quantification.

Co-immunoprecipitation and enrichment of glycosylated proteins

Precipitation experiments were done as described before [24, 50]: Cells were lysed in 1 ml lysis buffer (50 mM Tris, 2 mM $CaCl_2$, 137 mM NaCl, 2 mM EDTA, 10 mM 1,10-Phenanthroline, pH 7.5) supplemented with cOmplete™ protease inhibitor (Sigma; 11697498001). The lysates were cleared by centrifugation at 16,000 × g for 20 min at 4 °C. For the enrichment of glycosylated proteins, 450 µl of cleared lysate was incubated with 30 µl of Concanavalin A sepharose (Sigma; C9017). For co-immunoprecipitations (coIPs), 450 µl of cleared lysate was incubated with 10 µl of anti-HA magnetic beads (Thermo; 88836). The lysates were incubated with the beads for 90 min. Afterwards, the beads were washed five times with lysis buffer. The beads were heated in 40 µl reducing loading buffer (3% SDS, 16% glycerol, 8% 2-mercaptoethanol, 0.01% bromophenol blue, 0.1 M Tris HCl, pH 6.8) at 65 °C for 20 min.

Western blotting

Samples were subjected to SDS-PAGE and transferred onto PVDF membranes (Millipore, Immobilon-FL). Membranes were blocked with 5% non-fat dry milk in TBS (50 mM Tris, 150 mM NaCl, pH 7.4) for 20 min at room temperature. Primary antibodies were incubated overnight at 4 °C in 0.1% Tween-TBS and 1% BSA. After three washes with 0.1% Tween-TBS, membranes were incubated with a secondary antibody for 1 h at room temperature. Additional washing steps included one wash with 0.1% Tween-TBS and three washes with TBS. Protein detection was performed using the Odyssey 9120 imager system (LI-COR) and the ChemiDoc MP Imaging System (Bio-Rad). Band intensities were quantified using Image Studio Lite software (LI-COR). The following primary antibodies were used: αADAM17 (1:1000; Abcam; ab39162), αHA (1:2000; Biolegend; 901,502), αTransferrin-receptor (1:2000; Thermo, H68.4, 13-6800), αGAPDH (1:2000; Thermo, GA1R, 15738), αiRhom2 (1:1000; R&D; 996308; MAB10048), α14-3-3sigma (1:5000, Sigma, #PLA0201), α14-3-3pan (1:1000, Cell Signaling Technology, #8312S). The following secondary antibodies were used at the indicated dilutions: DyLight-680-conjugated αmouse (1:20,000; Thermo; 35519), DyLight-800-conjugated αrabbit (1:20,000; Thermo; 35,571), HRP-conjugated goat αmouse and αrabbit (1:20,000; Jackson ImmunoResearch Laboratories, Inc).

Shedding activity—AP-assay

ADAM17-mediated shedding activity was measured by an alkaline phosphatase (AP)–based assay as described before [24, 50]. In brief, we used cells transfected with ADAM17 substrates fused to an alkaline phosphatase to analyse shedding activity: The following ADAM17 substrates cloned in pCndA3.1 were utilised: AP-IL1R2, AP-TNFα, AP-AREG. HEK293 cells stably expressing the indicated iRhom2 constructs were transiently transfected with the indicated substrate. In the case of MEFs, the indicated iRhom2 construct combined with the indicated substrate was transiently transfected. Shedding activity was assessed under different conditions: either the metalloprotease inhibitors marimastat (broad-spectrum, 10 µM) (Sigma; M2699) or TAPI1 (ADAM17 preferential inhibitor, 10 µM) (Sigma; SML0739) were used. When indicated, cells were stimulated with 100 nM PMA (Sigma; P1585). DMSO served as the vehicle control. Following treatment, cells were incubated: 90 min (AREG, TGFα), 120 min (IL1R2), or 240 min (AREG) at 37 °C. To evaluate the proteolytic activity of ADAM17, we measured alkaline phosphatase (AP) activity in both the supernatant and cell lysates (lysis buffer: 50 mM Tris, 137 mM NaCl, 2 mM EDTA, 10 mM 1,10-phenanthroline, pH 7.5, supplemented with cOmplete™ protease inhibitor). By continuously measuring AP activity at 405 nm using the FLUOstar Optima (BMG LABTECH) after adding a p-nitrophenyl phosphate (PNPP) solution (Thermo; 37620), we calculated the slope representing the change in absorbance at 405 nm per min. ADAM17 activity was determined by calculating the PNPP substrate turnover (AP activity) in the supernatant relative to the total turnover in the supernatant plus cell lysate.

Flow cytometric analysis

The staining process was conducted using PBS with 0.2% BSA as the assay buffer, and all steps were carried out at 4 °C or on ice. A total of 2×10^5 cells of interest were incubated with the primary antibody for 1 h. Subsequently, cells were washed twice with 400 µl of assay buffer. The secondary antibody was added, and cells were incubated in the dark for 45 min. Following two additional washing steps, the fluorescence signal was assessed using flow cytometry (LSRFortessa, BD Biosciences, Heidelberg, Germany), and

FlowJo V10 software was employed for data analysis. The geometric mean of fluorescence intensity was determined to assess cell surface localisation. The primary antibodies used, along with their dilutions, were as follows: αADAM17 (1:100; R&D Systems; MAB 9301), αHA (1:500; Biolegend; 901502). The secondary antibody used was Allophycocyanin-conjugated αmouse (1:200; Jackson ImmunoResearch; 115-135-164).

Lysosomal inhibition

Cell cultures were first grown to approximately 80% confluence. Cells were treated with either bafilomycin A1 (B) or NH_4Cl (N). An untreated control was also included using DMSO as a vehicle control. The cells were then incubated for 8 h (B: 0.1 µM; N: 20 mM) or 16 h (B: 0.5 µM; N: 40 mM). After incubation, the plates were placed on ice and the medium was discarded. The cells were washed once with PBS and then harvested with 1 ml cold PBS. A 10 µl aliquot was taken from the cell suspension to determine the number of cells for sample adjustment. The harvested cells were centrifuged at 1000 g for 5 min at 4 °C and the supernatant was discarded. Cell pellets were used for lysis and coIPs followed by Western blotting as described above.

Cycloheximide-based pulse-chase experiment

Cell cultures were used at approximately 80% confluence. Cells were incubated with cycloheximide (10 µg/ml) for 3 or 6 h. After washing with PBS, the cells were harvested in 1 ml cold PBS and a 10 µl aliquot was taken from the cell suspension to determine the number of cells for sample adjustment. Harvested cells were pelleted and used for lysis followed by Western blotting as described above.

Statistics

The statistic was done as described before [24]: Experiments were repeated at least three times, as indicated in the figure legends. Quantitative data are presented as mean with standard deviation (SD). Statistical analysis was performed using the generalised mixed model analysis (PROC GLIMMIX, SAS 9.4, SAS Institute Inc., Cary, North Carolina, USA), assuming normal, lognormal, or beta distribution, with the day of the experiment considered as a random factor to assess treatment effect differences across the results. Diagnostic tests, including residual analysis and the Shapiro–Wilk test, were utilized. In cases of heteroscedasticity (as determined by the covtest statement), degrees of freedom were adjusted using the Kenward-Roger approximation. All p-values were adjusted for multiple comparisons using the false discovery rate (FDR). Statistical significance was defined as $p < 0.05$, with the following notation: p: * < 0.05, ** < 0.01, *** < 0.001.

Supplementary Information The online version contains supplementary material available at https://doi.org/10.1007/s00018-024-05132-3.

Acknowledgements We thank Johanna Jakob for cultivation of the primary cells.

Author contributions SD conceived, designed, and coordinated the study and wrote the manuscript. SD and AL analysed data and revised the manuscript. SD, KB, LL, SKT, CF, FS, SK, DK, CG, NT and XG performed experiments and analysed the results. SD conducted protein bioinformatics analysis, structure prediction and MD simulations. AB developed the algorithm for high-throughput identification of conserved regions and performed conservation analysis. SD and SK performed a meta-analysis of in vivo and ex vivo datasets. CA generated FRMD8/iTAP knock-out cells. SH and JMB isolated primary keratinocytes and fibroblasts. All authors read and approved the final version of the manuscript.

Funding Open Access funding enabled and organized by Projekt DEAL. To S.D. Research Fellowship of the German Research Foundation (280679981), ERS Start-up (StUpPD_299-18) and two START grants (#691903-06/19 and #692305- 06/23) of the Medical Faculty of the RWTH Aachen University. To A.L. funding from the German Research Foundation (418426903) and from the Interdisciplinary Centre for Clinical Research (IZKF) Aachen (A-1-5).

Availability of data and materials The datasets and materials generated during the current study are available from the corresponding author upon request.

Declarations

Conflict of interest The authors have no relevant financial or non-financial interests to disclose.

Ethics approval This study was conducted according to the principles of the Declaration of Helsinki and approved by the ethics committee of the Medical Faculty RWTH Aachen, Germany (EK 188/14).

Consent to participate Not applicable.

Consent for publication Not applicable.

Open Access This article is licensed under a Creative Commons Attribution 4.0 International License, which permits use, sharing, adaptation, distribution and reproduction in any medium or format, as long as you give appropriate credit to the original author(s) and the source, provide a link to the Creative Commons licence, and indicate if changes were made. The images or other third party material in this article are included in the article's Creative Commons licence, unless indicated otherwise in a credit line to the material. If material is not included in the article's Creative Commons licence and your intended use is not permitted by statutory regulation or exceeds the permitted use, you will need to obtain permission directly from the copyright holder. To view a copy of this licence, visit http://creativecommons.org/licenses/by/4.0/.

References

1. Abd Alla J, Graemer M, Fu X, Quitterer U (2016) Inhibition of G-protein-coupled receptor kinase 2 prevents the dysfunctional

cardiac substrate metabolism in fatty acid synthase transgenic mice. J Biol Chem 291(6):2583–2600. https://doi.org/10.1074/jbc.M115.702688
2. Adrain C, Zettl M, Christova Y, Taylor N, Freeman M (2012) Tumor necrosis factor signaling requires iRhom2 to promote trafficking and activation of TACE. Science 335(6065):225–228. https://doi.org/10.1126/science.1214400
3. Alcendor RR, Gao S, Zhai P, Zablocki D, Holle E, Yu X, Tian B, Wagner T, Vatner SF, Sadoshima J (2007) Sirt1 regulates aging and resistance to oxidative stress in the heart. Circ Res 100(10):1512–1521. https://doi.org/10.1161/01.RES.0000267723.65696.4a
4. Allende ML, Sipe LM, Tuymetova G, Wilson-Henjum KL, Chen W, Proia RL (2013) Sphingosine-1-phosphate phosphatase 1 regulates keratinocyte differentiation and epidermal homeostasis. J Biol Chem 288(25):18381–18391. https://doi.org/10.1074/jbc.M113.478420
5. Arakawa K, Hirose T, Inada T, Ito T, Kai T, Oyama M, Tomari Y, Yoda T, Nakagawa S (2023) Nondomain biopolymers: flexible molecular strategies to acquire biological functions. Genes Cells. https://doi.org/10.1111/gtc.13050
6. Arcidiacono P, Webb CM, Brooke MA, Zhou H, Delaney PJ, Ng KE, Blaydon DC, Tinker A, Kelsell DP, Chikh A (2018) p63 is a key regulator of iRHOM2 signalling in the keratinocyte stress response. Nat Commun 9(1):1021. https://doi.org/10.1038/s41467-018-03470-y
7. Arndt PG, Strahan B, Wang Y, Long C, Horiuchi K, Walcheck B (2011) Leukocyte ADAM17 regulates acute pulmonary inflammation. PLoS ONE 6(5):e19938. https://doi.org/10.1371/journal.pone.0019938
8. Babendreyer A, Rojas-Gonzalez DM, Giese AA, Fellendorf S, Düsterhöft S, Mela P, Ludwig A (2020) Differential induction of the ADAM17 regulators iRhom1 and 2 in endothelial cells. Front Cardiovasc Med 7:610344. https://doi.org/10.3389/fcvm.2020.610344
9. Barger JL, Kayo T, Vann JM, Arias EB, Wang J, Hacker TA, Wang Y, Raederstorff D, Morrow JD, Leeuwenburgh C, Allison DB, Saupe KW, Cartee GD, Weindruch R, Prolla TA (2008) A low dose of dietary resveratrol partially mimics caloric restriction and retards aging parameters in mice. PLoS ONE 3(6):e2264. https://doi.org/10.1371/journal.pone.0002264
10. Black RA, Rauch CT, Kozlosky CJ, Peschon JJ, Slack JL, Wolfson MF, Castner BJ, Stocking KL, Reddy P, Srinivasan S, Nelson N, Boiani N, Schooley KA, Gerhart M, Davis R, Fitzner JN, Johnson RS, Paxton RJ, March CJ, Cerretti DP (1997) A metalloproteinase disintegrin that releases tumour-necrosis factor-alpha from cells. Nature 385(6618):729–733. https://doi.org/10.1038/385729a0
11. Blaydon DC, Biancheri P, Di WL, Plagnol V, Cabral RM, Brooke MA, van Heel DA, Ruschendorf F, Toynbee M, Walne A, O'Toole EA, Martin JE, Lindley K, Vulliamy T, Abrams DJ, MacDonald TT, Harper JI, Kelsell DP (2011) Inflammatory skin and bowel disease linked to ADAM17 deletion. N Engl J Med 365(16):1502–1508. https://doi.org/10.1056/NEJMoa1100721
12. Blaydon DC, Etheridge SL, Risk JM, Hennies HC, Gay LJ, Carroll R, Plagnol V, McRonald FE, Stevens HP, Spurr NK, Bishop DT, Ellis A, Jankowski J, Field JK, Leigh IM, South AP, Kelsell DP (2012) RHBDF2 mutations are associated with tylosis, a familial esophageal cancer syndrome. Am J Hum Genet 90(2):340–346. https://doi.org/10.1016/j.ajhg.2011.12.008
13. Bosse Y, Maghni K, Hudson TJ (2007) 1alpha,25-dihydroxyvitamin D3 stimulation of bronchial smooth muscle cells induces autocrine, contractility, and remodeling processes. Physiol Genomics 29(2):161–168. https://doi.org/10.1152/physiolgenomics.00134.2006
14. Brooke MA, Etheridge SL, Kaplan N, Simpson C, O'Toole EA, Ishida-Yamamoto A, Marches O, Getsios S, Kelsell DP (2014) iRHOM2-dependent regulation of ADAM17 in cutaneous disease and epidermal barrier function. Hum Mol Genet 23(15):4064–4076. https://doi.org/10.1093/hmg/ddu120
15. Busch H, Camacho-Trullio D, Rogon Z, Breuhahn K, Angel P, Eils R, Szabowski A (2008) Gene network dynamics controlling keratinocyte migration. Mol Syst Biol 4:199. https://doi.org/10.1038/msb.2008.36
16. Cavadas M, Oikonomidi I, Gaspar CJ, Burbridge E, Badenes M, Felix I, Bolado A, Hu T, Bileck A, Gerner C, Domingos PM, von Kriegsheim A, Adrain C (2017) Phosphorylation of iRhom2 controls stimulated proteolytic shedding by the metalloprotease ADAM17/TACE. Cell Rep 21(3):745–757. https://doi.org/10.1016/j.celrep.2017.09.074
17. Chao-Chu J, Murtough S, Zaman N, Pennington DJ, Blaydon DC, Kelsell DP (2021) iRHOM2: a regulator of palmoplantar biology, inflammation, and viral susceptibility. J Invest Dermatol 141(4):722–726. https://doi.org/10.1016/j.jid.2020.09.010
18. Chen Y, Wei T, Yan L, Lawrence F, Qian HR, Burkholder TP, Starling JJ, Yingling JM, Shou J (2008) Developing and applying a gene functional association network for anti-angiogenic kinase inhibitor activity assessment in an angiogenesis co-culture model. BMC Genomics 9:264. https://doi.org/10.1186/1471-2164-9-264
19. Christova Y, Adrain C, Bambrough P, Ibrahim A, Freeman M (2013) Mammalian iRhoms have distinct physiological functions including an essential role in TACE regulation. EMBO Rep 14(10):884–890. https://doi.org/10.1038/embor.2013.128
20. Cock PJ, Antao T, Chang JT, Chapman BA, Cox CJ, Dalke A, Friedberg I, Hamelryck T, Kauff F, Wilczynski B, de Hoon MJ (2009) Biopython: freely available Python tools for computational molecular biology and bioinformatics. Bioinformatics 25(11):1422–1423. https://doi.org/10.1093/bioinformatics/btp163
21. Dosztanyi Z, Meszaros B, Simon I (2009) ANCHOR: web server for predicting protein binding regions in disordered proteins. Bioinformatics 25(20):2745–2746. https://doi.org/10.1093/bioinformatics/btp518
22. Dufour CR, Wilson BJ, Huss JM, Kelly DP, Alaynick WA, Downes M, Evans RM, Blanchette M, Giguere V (2007) Genome-wide orchestration of cardiac functions by the orphan nuclear receptors ERRalpha and gamma. Cell Metab 5(5):345–356. https://doi.org/10.1016/j.cmet.2007.03.007
23. Dulloo I, Tellier M, Levet C, Chikh A, Zhang B, Webb CM, Kelsell DP, Freeman M (2022) Cleavage of the pseudoprotease iRhom2 by the signal peptidase complex reveals an ER-to-nucleus signalling pathway. bioRxiv: 2022.2011.2028.518246 https://doi.org/10.1101/2022.11.28.518246
24. Düsterhöft S, Kahveci-Turkoz S, Wozniak J, Seifert A, Kasparek P, Ohm H, Liu S, Kopkanova J, Lokau J, Garbers C, Preisinger C, Sedlacek R, Freeman M, Ludwig A (2021) The iRhom homology domain is indispensable for ADAM17-mediated TNFalpha and EGF receptor ligand release. Cell Mol Life Sci. https://doi.org/10.1007/s00018-021-03845-3
25. Düsterhöft S, Lokau J, Garbers C (2019) The metalloprotease ADAM17 in inflammation and cancer. Pathol Res Pract 215(6):152410. https://doi.org/10.1016/j.prp.2019.04.002
26. Dyson HJ (2016) Making sense of intrinsically disordered proteins. Biophys J 110(5):1013–1016. https://doi.org/10.1016/j.bpj.2016.01.030
27. Ellis A, Field JK, Field EA, Friedmann PS, Fryer A, Howard P, Leigh IM, Risk J, Shaw JM, Whittaker J (1994) Tylosis associated with carcinoma of the oesophagus and oral leukoplakia in a large Liverpool family–a review of six generations. Eur J

Cancer B Oral Oncol 30B(2):102–112. https://doi.org/10.1016/0964-1955(94)90061-2
28. Ellis A, Risk JM, Maruthappu T, Kelsell DP (2015) Tylosis with oesophageal cancer: diagnosis, management and molecular mechanisms. Orphanet J Rare Dis 10:126. https://doi.org/10.1186/s13023-015-0346-2
29. Erdos G, Pajkos M, Dosztanyi Z (2021) IUPred3: prediction of protein disorder enhanced with unambiguous experimental annotation and visualization of evolutionary conservation. Nucleic Acids Res 49(W1):W297–W303. https://doi.org/10.1093/nar/gkab408
30. Esaki H, Ewald DA, Ungar B, Rozenblit M, Zheng X, Xu H, Estrada YD, Peng X, Mitsui H, Litman T, Suarez-Farinas M, Krueger JG, Guttman-Yassky E (2015) Identification of novel immune and barrier genes in atopic dermatitis by means of laser capture microdissection. J Allergy Clin Immunol 135(1):153–163. https://doi.org/10.1016/j.jaci.2014.10.037
31. Gambino V, De Michele G, Venezia O, Migliaccio P, Dall'Olio V, Bernard L, Minardi SP, Della Fazia MA, Bartoli D, Servillo G, Alcalay M, Luzi L, Giorgio M, Scrable H, Pelicci PG, Migliaccio E (2013) Oxidative stress activates a specific p53 transcriptional response that regulates cellular senescence and aging. Aging Cell 12(3):435–445. https://doi.org/10.1111/acel.12060
32. Garinis GA, Uittenboogaard LM, Stachelscheid H, Fousteri M, van Ijcken W, Breit TM, van Steeg H, Mullenders LH, van der Horst GT, Bruning JC, Niessen CM, Hoeijmakers JH, Schumacher B (2009) Persistent transcription-blocking DNA lesions trigger somatic growth attenuation associated with longevity. Nat Cell Biol 11(5):604–615. https://doi.org/10.1038/ncb1866
33. Giese AA, Babendreyer A, Krappen P, Gross A, Strnad P, Düsterhöft S, Ludwig A (2021) Inflammatory activation of surface molecule shedding by upregulation of the pseudoprotease iRhom2 in colon epithelial cells. Sci Rep 11(1):24230. https://doi.org/10.1038/s41598-021-03522-2
34. Grieve A, Xu H, Künzel U, Bambrough P, Sieber B, Freeman M (2017) Phosphorylation of iRhom2 at the plasma membrane controls mammalian TACE-dependent inflammatory and growth factor signalling. Elife. https://doi.org/10.7554/eLife.23968
35. Guo A, Gu H, Zhou J, Mulhern D, Wang Y, Lee KA, Yang V, Aguiar M, Kornhauser J, Jia X, Ren J, Beausoleil SA, Silva JC, Vemulapalli V, Bedford MT, Comb MJ (2014) Immunoaffinity enrichment and mass spectrometry analysis of protein methylation. Mol Cell Proteomics 13(1):372–387. https://doi.org/10.1074/mcp.O113.027870
36. Henrichsen CN, Csardi G, Zabot MT, Fusco C, Bergmann S, Merla G, Reymond A (2011) Using transcription modules to identify expression clusters perturbed in Williams-Beuren syndrome. PLoS Comput Biol 7(1):e1001054. https://doi.org/10.1371/journal.pcbi.1001054
37. Ho SN, Hunt HD, Horton RM, Pullen JK, Pease LR (1989) Site-directed mutagenesis by overlap extension using the polymerase chain reaction. Gene 77(1):51–59. https://doi.org/10.1016/0378-1119(89)90358-2
38. Hornbeck PV, Zhang B, Murray B, Kornhauser JM, Latham V, Skrzypek E (2015) PhosphoSitePlus, 2014: mutations, PTMs and recalibrations. Nucleic Acids Res 43:D512-520. https://doi.org/10.1093/nar/gku1267
39. Hosur V, Farley ML, Burzenski LM, Shultz LD, Wiles MV (2018) ADAM17 is essential for ectodomain shedding of the EGF-receptor ligand amphiregulin. FEBS Open Bio 8(4):702–710. https://doi.org/10.1002/2211-5463.12407
40. Hosur V, Farley ML, Low BE, Burzenski LM, Shultz LD, Wiles MV (2018) RHBDF2-regulated growth factor signaling in a rare human disease, tylosis with esophageal cancer: what can we learn from murine models? Front Genet 9:233. https://doi.org/10.3389/fgene.2018.00233
41. Hosur V, Johnson KR, Burzenski LM, Stearns TM, Maser RS, Shultz LD (2014) Rhbdf2 mutations increase its protein stability and drive EGFR hyperactivation through enhanced secretion of amphiregulin. Proc Natl Acad Sci U S A 111(21):E2200-2209. https://doi.org/10.1073/pnas.1323908111
42. Hosur V, Low BE, Shultz LD, Wiles MV (2017) Genetic deletion of amphiregulin restores the normal skin phenotype in a mouse model of the human skin disease tylosis. Biol Open 6(8):1174–1179. https://doi.org/10.1242/bio.026260
43. Howel-Evans W, Mc CR, Clarke CA, Sheppard PM (1958) Carcinoma of the oesophagus with keratosis palmaris et plantaris (tylosis): a study of two families. Q J Med 27(107):413–429
44. Hruz T, Laule O, Szabo G, Wessendorp F, Bleuler S, Oertle L, Widmayer P, Gruissem W, Zimmermann P (2008) Genevestigator v3: a reference expression database for the meta-analysis of transcriptomes. Adv Bioinformatics 2008:420747. https://doi.org/10.1155/2008/420747
45. Inada M, Izawa G, Kobayashi W, Ozawa M (2016) 293 cells express both epithelial as well as mesenchymal cell adhesion molecules. Int J Mol Med 37(6):1521–1527. https://doi.org/10.3892/ijmm.2016.2568
46. Issuree PD, Maretzky T, McIlwain DR, Monette S, Qing X, Lang PA, Swendeman SL, Park-Min KH, Binder N, Kalliolias GD, Yarilina A, Horiuchi K, Ivashkiv LB, Mak TW, Salmon JE, Blobel CP (2013) iRHOM2 is a critical pathogenic mediator of inflammatory arthritis. J Clin Invest 123(2):928–932. https://doi.org/10.1172/JCI66168
47. Jocher G, Grass V, Tschirner SK, Riepler L, Breimann S, Kaya T, Oelsner M, Hamad MS, Hofmann LI, Blobel CP, Schmidt-Weber CB, Gokce O, Jakwerth CA, Trimpert J, Kimpel J, Pichlmair A, Lichtenthaler SF (2022) ADAM10 and ADAM17 promote SARS-CoV-2 cell entry and spike protein-mediated lung cell fusion. EMBO Rep 23(6):e54305. https://doi.org/10.15252/embr.202154305
48. Johnson KR, Lane PW, Cook SA, Harris BS, Ward-Bailey PF, Bronson RT, Lyons BL, Shultz LD, Davisson MT (2003) Curly bare (cub), a new mouse mutation on chromosome 11 causing skin and hair abnormalities, and a modifier gene (mcub) on chromosome 5. Genomics 81(1):6–14. https://doi.org/10.1016/S0888-7543(02)00013-7
49. Jumper J, Evans R, Pritzel A, Green T, Figurnov M, Ronneberger O, Tunyasuvunakool K, Bates R, Zidek A, Potapenko A, Bridgland A, Meyer C, Kohl SAA, Ballard AJ, Cowie A, Romera-Paredes B, Nikolov S, Jain R, Adler J, Back T, Petersen S, Reiman D, Clancy E, Zielinski M, Steinegger M, Pacholska M, Berghammer T, Bodenstein S, Silver D, Vinyals O, Senior AW, Kavukcuoglu K, Kohli P, Hassabis D (2021) Highly accurate protein structure prediction with AlphaFold. Nature 596(7873):583–589. https://doi.org/10.1038/s41586-021-03819-2
50. Kahveci-Türköz S, Bläsius K, Wozniak J, Rinkens C, Seifert A, Kasparek P, Ohm H, Oltzen S, Nieszporek M, Schwarz N, Babendreyer A, Preisinger C, Sedlacek R, Ludwig A, Düsterhöft S (2023) A structural model of the iRhom-ADAM17 sheddase complex reveals functional insights into its trafficking and activity. Cell Mol Life Sci 80(5):135. https://doi.org/10.1007/s00018-023-04783-y
51. Ketteler R, Glaser S, Sandra O, Martens UM, Klingmuller U (2002) Enhanced transgene expression in primitive hematopoietic progenitor cells and embryonic stem cells efficiently transduced by optimized retroviral hybrid vectors. Gene Ther 9(8):477–487. https://doi.org/10.1038/sj.gt.3301653
52. Klausen MS, Jespersen MC, Nielsen H, Jensen KK, Jurtz VI, Sonderby CK, Sommer MOA, Winther O, Nielsen M, Petersen B, Marcatili P (2019) NetSurfP-2.0: improved prediction of protein structural features by integrated deep learning. Proteins 87(6):520–527. https://doi.org/10.1002/prot.25674

53. Ku NO, Michie S, Resurreccion EZ, Broome RL, Omary MB (2002) Keratin binding to 14-3-3 proteins modulates keratin filaments and hepatocyte mitotic progression. Proc Natl Acad Sci U S A 99(7):4373–4378. https://doi.org/10.1073/pnas.072624299
54. Kubo S, Fritz JM, Raquer-McKay HM, Kataria R, Vujkovic-Cvijin I, Al-Shaibi A, Yao Y, Zheng L, Zou J, Waldman AD, Jing X, Farley TK, Park AY, Oler AJ, Charles AK, Makhlouf M, Abou-Moussa EH, Hasnah R, Saraiva LR, Ganesan S, Al-Subaiey AA, Matthews H, Flano E, Lee HH, Freeman AF, Sefer AP, Sayar E, Cakir E, Karakoc-Aydiner E, Baris S, Belkaid Y, Ozen A, Lo B, Lenardo MJ (2022) Congenital iRHOM2 deficiency causes ADAM17 dysfunction and environmentally directed immunodysregulatory disease. Nat Immunol 23(1):75–85. https://doi.org/10.1038/s41590-021-01093-y
55. Künzel U, Grieve AG, Meng Y, Sieber B, Cowley SA, Freeman M (2018) FRMD8 promotes inflammatory and growth factor signalling by stabilising the iRhom/ADAM17 sheddase complex. Elife. https://doi.org/10.7554/eLife.35012
56. Lambert DW, Yarski M, Warner FJ, Thornhill P, Parkin ET, Smith AI, Hooper NM, Turner AJ (2005) Tumor necrosis factor-alpha convertase (ADAM17) mediates regulated ectodomain shedding of the severe-acute respiratory syndrome-coronavirus (SARS-CoV) receptor, angiotensin-converting enzyme-2 (ACE2). J Biol Chem 280(34):30113–30119. https://doi.org/10.1074/jbc.M505111200
57. Lattin JE, Schroder K, Su AI, Walker JR, Zhang J, Wiltshire T, Saijo K, Glass CK, Hume DA, Kellie S, Sweet MJ (2008) Expression analysis of G Protein-Coupled Receptors in mouse macrophages. Immunome Res 4:5. https://doi.org/10.1186/1745-7580-4-5
58. Li X, Maretzky T, Perez-Aguilar JM, Monette S, Weskamp G, Le Gall S, Beutler B, Weinstein H, Blobel CP (2017) Structural modeling defines transmembrane residues in ADAM17 that are crucial for Rhbdf2-ADAM17-dependent proteolysis. J Cell Sci 130(5):868–878. https://doi.org/10.1242/jcs.196436
59. Li X, Maretzky T, Weskamp G, Monette S, Qing X, Issuree PD, Crawford HC, McIlwain DR, Mak TW, Salmon JE, Blobel CP (2015) iRhoms 1 and 2 are essential upstream regulators of ADAM17-dependent EGFR signaling. Proc Natl Acad Sci U S A 112(19):6080–6085. https://doi.org/10.1073/pnas.1505649112
60. Lindorff-Larsen K, Piana S, Palmo K, Maragakis P, Klepeis JL, Dror RO, Shaw DE (2010) Improved side-chain torsion potentials for the Amber ff99SB protein force field. Proteins 78(8):1950–1958. https://doi.org/10.1002/prot.22711
61. Lu XL, Zhao CH, Zhang H, Yao XL (2017) iRhom2 is involved in lipopolysaccharide-induced cardiac injury in vivo and in vitro through regulating inflammation response. Biomed Pharmacother 86:645–653. https://doi.org/10.1016/j.biopha.2016.11.075
62. Lucas E, Jurado-Pueyo M, Fortuno MA, Fernandez-Veledo S, Vila-Bedmar R, Jimenez-Borreguero LJ, Lazcano JJ, Gao E, Gomez-Ambrosi J, Fruhbeck G, Koch WJ, Diez J, Mayor F Jr, Murga C (2014) Downregulation of G protein-coupled receptor kinase 2 levels enhances cardiac insulin sensitivity and switches on cardioprotective gene expression patterns. Biochim Biophys Acta 1842(12 Pt A):2448–2456. https://doi.org/10.1016/j.bbadis.2014.09.004
63. Maney SK, McIlwain DR, Polz R, Pandyra AA, Sundaram B, Wolff D, Ohishi K, Maretzky T, Brooke MA, Evers A, Vasudevan AA, Aghaeepour N, Scheller J, Munk C, Haussinger D, Mak TW, Nolan GP, Kelsell DP, Blobel CP, Lang KS, Lang PA (2015) Deletions in the cytoplasmic domain of iRhom1 and iRhom2 promote shedding of the TNF receptor by the protease ADAM17. Sci Signal 8(401):ra109. https://doi.org/10.1126/scisignal.aac5356
64. Marchina E, Misasi S, Bozzato A, Ferraboli S, Agosti C, Rozzini L, Borsani G, Barlati S, Padovani A (2014) Gene expression profile in fibroblasts of Huntington's disease patients and controls. J Neurol Sci 337(1–2):42–46. https://doi.org/10.1016/j.jns.2013.11.014
65. Maretzky T, McIlwain DR, Issuree PD, Li X, Malapeira J, Amin S, Lang PA, Mak TW, Blobel CP (2013) iRhom2 controls the substrate selectivity of stimulated ADAM17-dependent ectodomain shedding. Proc Natl Acad Sci U S A 110(28):11433–11438. https://doi.org/10.1073/pnas.1302553110
66. Maruthappu T, Chikh A, Fell B, Delaney PJ, Brooke MA, Levet C, Moncada-Pazos A, Ishida-Yamamoto A, Blaydon D, Waseem A, Leigh IM, Freeman M, Kelsell DP (2017) Rhomboid family member 2 regulates cytoskeletal stress-associated Keratin 16. Nat Commun 8:14174. https://doi.org/10.1038/ncomms14174
67. McIlwain DR, Lang PA, Maretzky T, Hamada K, Ohishi K, Maney SK, Berger T, Murthy A, Duncan G, Xu HC, Lang KS, Haussinger D, Wakeham A, Itie-Youten A, Khokha R, Ohashi PS, Blobel CP, Mak TW (2012) iRhom2 regulation of TACE controls TNF-mediated protection against Listeria and responses to LPS. Science 335(6065):229–232. https://doi.org/10.1126/science.1214448
68. Mercader JM, Puiggros M, Segre AV, Planet E, Sorianello E, Sebastian D, Rodriguez-Cuenca S, Ribas V, Bonas-Guarch S, Draghici S, Yang C, Mora S, Vidal-Puig A, Dupuis J, Florez JC, Zorzano A, Torrents D (2012) Identification of novel type 2 diabetes candidate genes involved in the crosstalk between the mitochondrial and the insulin signaling systems. PLoS Genet 8(12):e1003046. https://doi.org/10.1371/journal.pgen.1003046
69. Meszaros B, Erdos G, Dosztanyi Z (2018) IUPred2A: context-dependent prediction of protein disorder as a function of redox state and protein binding. Nucleic Acids Res 46(W1):W329–W337. https://doi.org/10.1093/nar/gky384
70. Meszaros B, Simon I, Dosztanyi Z (2009) Prediction of protein binding regions in disordered proteins. PLoS Comput Biol 5(5):e1000376. https://doi.org/10.1371/journal.pcbi.1000376
71. Mirdita M, Schutze K, Moriwaki Y, Heo L, Ovchinnikov S, Steinegger M (2022) ColabFold: making protein folding accessible to all. Nat Methods 19(6):679–682. https://doi.org/10.1038/s41592-022-01488-1
72. Mokoena T, Smit JGM, Karusseit VO, Dorfling CM, van Rensburg EJ (2018) Tylosis associated with squamous cell carcinoma of the oesophagus (TOC): report of an African family with a novel RHBDF2 variant. Clin Genet 93(5):1114–1116. https://doi.org/10.1111/cge.13161
73. Muchir A, Pavlidis P, Bonne G, Hayashi YK, Worman HJ (2007) Activation of MAPK in hearts of EMD null mice: similarities between mouse models of X-linked and autosomal dominant Emery Dreifuss muscular dystrophy. Hum Mol Genet 16(15):1884–1895. https://doi.org/10.1093/hmg/ddm137
74. Nguyen Ba AN, Pogoutse A, Provart N, Moses AM (2009) NLStradamus: a simple Hidden Markov Model for nuclear localization signal prediction. BMC Bioinformatics 10:202. https://doi.org/10.1186/1471-2105-10-202
75. Niehues RV, Wozniak J, Wiersch F, Lilienthal E, Tacken N, Schumertl T, Garbers C, Ludwig A, Düsterhöft S (2022) The collectrin-like part of the SARS-CoV-1 and -2 receptor ACE2 is shed by the metalloproteinases ADAM10 and ADAM17. FASEB J 36(3):e22234. https://doi.org/10.1096/fj.202101521R
76. Obsilova V, Obsil T (2022) Structural insights into the functional roles of 14-3-3 proteins. Front Mol Biosci 9:1016071. https://doi.org/10.3389/fmolb.2022.1016071
77. Oikonomidi I, Burbridge E, Cavadas M, Sullivan G, Collis B, Naegele H, Clancy D, Brezinova J, Hu T, Bileck A, Gerner C, Bolado A, von Kriegsheim A, Martin SJ, Steinberg F, Strisovsky K, Adrain C (2018) iTAP, a novel iRhom interactor, controls

TNF secretion by policing the stability of iRhom/TACE. Elife. https://doi.org/10.7554/eLife.35032
78. Oka S, Alcendor R, Zhai P, Park JY, Shao D, Cho J, Yamamoto T, Tian B, Sadoshima J (2011) PPARalpha-Sirt1 complex mediates cardiac hypertrophy and failure through suppression of the ERR transcriptional pathway. Cell Metab 14(5):598–611. https://doi.org/10.1016/j.cmet.2011.10.001
79. Palau V, Riera M, Soler MJ (2020) ADAM17 inhibition may exert a protective effect on COVID-19. Nephrol Dial Transplant 35(6):1071–1072. https://doi.org/10.1093/ndt/gfaa093
80. Peschon JJ, Slack JL, Reddy P, Stocking KL, Sunnarborg SW, Lee DC, Russell WE, Castner BJ, Johnson RS, Fitzner JN, Boyce RW, Nelson N, Kozlosky CJ, Wolfson MF, Rauch CT, Cerretti DP, Paxton RJ, March CJ, Black RA (1998) An essential role for ectodomain shedding in mammalian development. Science 282(5392):1281–1284. https://doi.org/10.1126/science.282.5392.1281
81. Pettersen EF, Goddard TD, Huang CC, Meng EC, Couch GS, Croll TI, Morris JH, Ferrin TE (2021) UCSF ChimeraX: structure visualization for researchers, educators, and developers. Protein Sci 30(1):70–82. https://doi.org/10.1002/pro.3943
82. Pronk S, Pall S, Schulz R, Larsson P, Bjelkmar P, Apostolov R, Shirts MR, Smith JC, Kasson PM, van der Spoel D, Hess B, Lindahl E (2013) GROMACS 4.5: a high-throughput and highly parallel open source molecular simulation toolkit. Bioinformatics 29(7):845–854. https://doi.org/10.1093/bioinformatics/btt055
83. Qu L, Sha S, Zou QL, Gao XH, Xiao T, Chen HD, He CC (2019) Whole exome sequencing identified a novel mutation of the RHBDF2 gene in a chinese family of tylosis with esophageal cancer. Acta Derm Venereol 99(7):699–700. https://doi.org/10.2340/00015555-3189
84. Rabinowitsch AI, Maretzky T, Weskamp G, Haxaire C, Tueshaus J, Lichtenthaler SF, Monette S, Blobel CP (2023) Analysis of the function of ADAM17 in iRhom2-curly-bare (cub) and Tylosis with Oesophageal Cancer (TOC) mutant mice. J Cell Sci. https://doi.org/10.1242/jcs.260910
85. Ramchandran R, Takezako T, Saad Y, Stull L, Fink B, Yamada H, Dikalov S, Harrison DG, Moravec C, Karnik SS (2006) Angiotensinergic stimulation of vascular endothelium in mice causes hypotension, bradycardia, and attenuated angiotensin response. Proc Natl Acad Sci U S A 103(50):19087–19092. https://doi.org/10.1073/pnas.0602715103
86. Ricard G, Molina J, Chrast J, Gu W, Gheldof N, Pradervand S, Schutz F, Young JI, Lupski JR, Reymond A, Walz K (2010) Phenotypic consequences of copy number variation: insights from Smith-Magenis and Potocki-Lupski syndrome mouse models. PLoS Biol 8(11):e1000543. https://doi.org/10.1371/journal.pbio.1000543
87. Rizza S, Copetti M, Cardellini M, Menghini R, Pecchioli C, Luzi A, Di Cola G, Porzio O, Ippoliti A, Romeo F, Pellegrini F, Federici M (2015) A score including ADAM17 substrates correlates to recurring cardiovascular event in subjects with atherosclerosis. Atherosclerosis 239(2):459–464. https://doi.org/10.1016/j.atherosclerosis.2015.01.029
88. Roth RB, Hevezi P, Lee J, Willhite D, Lechner SM, Foster AC, Zlotnik A (2006) Gene expression analyses reveal molecular relationships among 20 regions of the human CNS. Neurogenetics 7(2):67–80. https://doi.org/10.1007/s10048-006-0032-6
89. Ruijter JM, Ramakers C, Hoogaars WM, Karlen Y, Bakker O, van den Hoff MJ, Moorman AF (2009) Amplification efficiency: linking baseline and bias in the analysis of quantitative PCR data. Nucleic Acids Res 37(6):e45. https://doi.org/10.1093/nar/gkp045
90. Sa SM, Valdez PA, Wu J, Jung K, Zhong F, Hall L, Kasman I, Winer J, Modrusan Z, Danilenko DM, Ouyang W (2007) The effects of IL-20 subfamily cytokines on reconstituted human epidermis suggest potential roles in cutaneous innate defense and pathogenic adaptive immunity in psoriasis. J Immunol 178(4):2229–2240. https://doi.org/10.4049/jimmunol.178.4.2229
91. Saarinen S, Vahteristo P, Lehtonen R, Aittomaki K, Launonen V, Kiviluoto T, Aaltonen LA (2012) Analysis of a Finnish family confirms RHBDF2 mutations as the underlying factor in tylosis with esophageal cancer. Fam Cancer 11(3):525–528. https://doi.org/10.1007/s10689-012-9532-8
92. Sahin U, Weskamp G, Kelly K, Zhou HM, Higashiyama S, Peschon J, Hartmann D, Saftig P, Blobel CP (2004) Distinct roles for ADAM10 and ADAM17 in ectodomain shedding of six EGFR ligands. J Cell Biol 164(5):769–779. https://doi.org/10.1083/jcb.200307137
93. Sato T, Kaneda A, Tsuji S, Isagawa T, Yamamoto S, Fujita T, Yamanaka R, Tanaka Y, Nukiwa T, Marquez VE, Ishikawa Y, Ichinose M, Aburatani H (2013) PRC2 overexpression and PRC2-target gene repression relating to poorer prognosis in small cell lung cancer. Sci Rep 3:1911. https://doi.org/10.1038/srep01911
94. Schmitt L, Huth S, Amann PM, Marquardt Y, Heise R, Fietkau K, Huth L, Steiner T, Holzle F, Baron JM (2018) Direct biological effects of fractional ultrapulsed CO(2) laser irradiation on keratinocytes and fibroblasts in human organotypic full-thickness 3D skin models. Lasers Med Sci 33(4):765–772. https://doi.org/10.1007/s10103-017-2409-1
95. Schumacher N, Thomsen I, Brundert F, Hejret V, Düsterhöft S, Tichy B, Schmidt-Arras D, Voss M, Rose-John S (2023) EGFR stimulation enables IL-6 trans-signalling via iRhom2-dependent ADAM17 activation in mammary epithelial cells. Biochim Biophys Acta Mol Cell Res. https://doi.org/10.1016/j.bbamcr.2023.119489
96. Shalhoub V, Shatzen EM, Ward SC, Young JI, Boedigheimer M, Twehues L, McNinch J, Scully S, Twomey B, Baker D, Kiaei P, Damore MA, Pan Z, Haas K, Martin D (2010) Chondro/osteoblastic and cardiovascular gene modulation in human artery smooth muscle cells that calcify in the presence of phosphate and calcitriol or paricalcitol. J Cell Biochem 111(4):911–921. https://doi.org/10.1002/jcb.22779
97. Shuai Y, Guo J, Dong Y, Zhong W, Xiao P, Zhou T, Zhang L, Peng S (2011) Global gene expression profiles of MT knockout and wild-type mice in the condition of doxorubicin-induced cardiomyopathy. Toxicol Lett 200(1–2):77–87. https://doi.org/10.1016/j.toxlet.2010.10.017
98. Sieber B, Lu F, Stribbling SM, Grieve AG, Ryan AJ, Freeman M (2022) iRhom2 regulates ERBB signalling to promote KRAS-driven tumour growth of lung cancer cells. J Cell Sci. https://doi.org/10.1242/jcs.259949
99. Sievers F, Wilm A, Dineen D, Gibson TJ, Karplus K, Li W, Lopez R, McWilliam H, Remmert M, Soding J, Thompson JD, Higgins DG (2011) Fast, scalable generation of high-quality protein multiple sequence alignments using Clustal Omega. Mol Syst Biol 7:539. https://doi.org/10.1038/msb.2011.75
100. Siggs OM, Grieve A, Xu H, Bambrough P, Christova Y, Freeman M (2014) Genetic interaction implicates iRhom2 in the regulation of EGF receptor signalling in mice. Biol Open 3(12):1151–1157. https://doi.org/10.1242/bio.201410116
101. Siggs OM, Xiao N, Wang Y, Shi H, Tomisato W, Li X, Xia Y, Beutler B (2012) iRhom2 is required for the secretion of mouse TNFalpha. Blood 119(24):5769–5771. https://doi.org/10.1182/blood-2012-03-417949
102. Smith JC, Boone BE, Opalenik SR, Williams SM, Russell SB (2008) Gene profiling of keloid fibroblasts shows altered expression in multiple fibrosis-associated pathways. J Invest Dermatol 128(5):1298–1310. https://doi.org/10.1038/sj.jid.5701149
103. Smyth EC, Lagergren J, Fitzgerald RC, Lordick F, Shah MA, Lagergren P, Cunningham D (2017) Oesophageal cancer. Nat Rev Dis Primers 3:17048. https://doi.org/10.1038/nrdp.2017.48

104. Strunnikova NV, Barb J, Sergeev YV, Thiagarajasubramanian A, Silvin C, Munson PJ, Macdonald IM (2009) Loss-of-function mutations in Rab escort protein 1 (REP-1) affect intracellular transport in fibroblasts and monocytes of choroideremia patients. PLoS ONE 4(12):e8402. https://doi.org/10.1371/journal.pone.0008402
105. Swindell WR, Xing X, Stuart PE, Chen CS, Aphale A, Nair RP, Voorhees JJ, Elder JT, Johnston A, Gudjonsson JE (2012) Heterogeneity of inflammatory and cytokine networks in chronic plaque psoriasis. PLoS ONE 7(3):e34594. https://doi.org/10.1371/journal.pone.0034594
106. Tang B, Li X, Maretzky T, Perez-Aguilar JM, McIlwain D, Xie Y, Zheng Y, Mak TW, Weinstein H, Blobel CP (2020) Substrate-selective protein ectodomain shedding by ADAM17 and iRhom2 depends on their juxtamembrane and transmembrane domains. FASEB J 34(4):4956–4969. https://doi.org/10.1096/fj.201902649R
107. Thorrez L, Van Deun K, Tranchevent LC, Van Lommel L, Engelen K, Marchal K, Moreau Y, Van Mechelen I, Schuit F (2008) Using ribosomal protein genes as reference: a tale of caution. PLoS ONE 3(3):e1854. https://doi.org/10.1371/journal.pone.0001854
108. Traister A, Walsh M, Aafaqi S, Lu M, Dai X, Henkleman MR, Momen A, Zhou YQ, Husain M, Arab S, Piran S, Hannigan G, Coles JG (2013) Mutation in integrin-linked kinase (ILK(R211A)) and heat-shock protein 70 comprise a broadly cardioprotective complex. PLoS ONE 8(11):e77331. https://doi.org/10.1371/journal.pone.0077331
109. Uhlenhopp DJ, Then EO, Sunkara T, Gaduputi V (2020) Epidemiology of esophageal cancer: update in global trends, etiology and risk factors. Clin J Gastroenterol 13(6):1010–1021. https://doi.org/10.1007/s12328-020-01237-x
110. Vallender TW, Lahn BT (2006) Localized methylation in the key regulator gene endothelin-1 is associated with cell type-specific transcriptional silencing. FEBS Lett 580(18):4560–4566. https://doi.org/10.1016/j.febslet.2006.07.017
111. Van Durme J, Delgado J, Stricher F, Serrano L, Schymkowitz J, Rousseau F (2011) A graphical interface for the FoldX forcefield. Bioinformatics 27(12):1711–1712. https://doi.org/10.1093/bioinformatics/btr254
112. Verkerk AJ, Schot R, Dumee B, Schellekens K, Swagemakers S, Bertoli-Avella AM, Lequin MH, Dudink J, Govaert P, van Zwol AL, Hirst J, Wessels MW, Catsman-Berrevoets C, Verheijen FW, de Graaff E, de Coo IF, Kros JM, Willemsen R, Willems PJ, van der Spek PJ, Mancini GM (2009) Mutation in the AP4M1 gene provides a model for neuroaxonal injury in cerebral palsy. Am J Hum Genet 85(1):40–52. https://doi.org/10.1016/j.ajhg.2009.06.004
113. Visser R, Landman EB, Goeman J, Wit JM, Karperien M (2012) Sotos syndrome is associated with deregulation of the MAPK/ERK-signaling pathway. PLoS ONE 7(11):e49229. https://doi.org/10.1371/journal.pone.0049229
114. Voets AM, Huigsloot M, Lindsey PJ, Leenders AM, Koopman WJ, Willems PH, Rodenburg RJ, Smeitink JA, Smeets HJ (2012) Transcriptional changes in OXPHOS complex I deficiency are related to anti-oxidant pathways and could explain the disturbed calcium homeostasis. Biochim Biophys Acta 1822(7):1161–1168. https://doi.org/10.1016/j.bbadis.2011.10.009
115. Wang L, Zhang TP, Zhang Y, Bi HL, Guan XM, Wang HX, Wang X, Du J, Xia YL, Li HH (2016) Protection against doxorubicin-induced myocardial dysfunction in mice by cardiac-specific expression of carboxyl terminus of hsp70-interacting protein. Sci Rep 6:28399. https://doi.org/10.1038/srep28399
116. Wang Q, Ma C, Kemmner W (2013) Wdr66 is a novel marker for risk stratification and involved in epithelial-mesenchymal transition of esophageal squamous cell carcinoma. BMC Cancer 13:137. https://doi.org/10.1186/1471-2407-13-137
117. Wang XM, Yik WY, Zhang P, Lu W, Dranchak PK, Shibata D, Steinberg SJ, Hacia JG (2012) The gene expression profiles of induced pluripotent stem cells from individuals with childhood cerebral adrenoleukodystrophy are consistent with proposed mechanisms of pathogenesis. Stem Cell Res Ther 3(5):39. https://doi.org/10.1186/scrt130
118. Wong J, Chang C, Agrawal R, Walton GB, Chen C, Murthy A, Patterson AJ (2010) Gene expression profiling: classification of mice with left ventricle systolic dysfunction using microarray analysis. Crit Care Med 38(1):25–31. https://doi.org/10.1097/CCM.0b013e3181b427e8
119. Yang T, Hui R, Nouws J, Sauler M, Zeng T, Wu Q (2022) Untargeted metabolomics analysis of esophageal squamous cell cancer progression. J Transl Med 20(1):127. https://doi.org/10.1186/s12967-022-03311-z
120. Yuan F, Li D, Li C, Zhang Y, Song H, Li S, Deng H, Gao GF, Zheng A (2021) ADAM17 is an essential attachment factor for classical swine fever virus. PLoS Pathog 17(3):e1009393. https://doi.org/10.1371/journal.ppat.1009393
121. Yunoki T, Tabuchi Y, Hirano T, Miwa S, Imura J, Hayashi A (2018) Gene networks in basal cell carcinoma of the eyelid, analyzed using gene expression profiling. Oncol Lett 16(5):6729–6734. https://doi.org/10.3892/ol.2018.9484
122. Zanotti A, Coelho JPL, Kaylani D, Singh G, Tauber M, Hitzenberger M, Avci D, Zacharias M, Russell RB, Lemberg MK, Feige MJ (2022) The human signal peptidase complex acts as a quality control enzyme for membrane proteins. Science 378(6623):996–1000. https://doi.org/10.1126/science.abo5672
123. Zaruba M, Chen HW, Pietsch OF, Szakmary-Braendle K, Auer A, Motz M, Seitz K, Düsterhöft S, Workman AM, Rumenapf T, Riedel C (2022) ADAM17 is an essential factor for the infection of bovine cells with pestiviruses. Viruses. https://doi.org/10.3390/v14020381
124. Zhao Y, Ransom JF, Li A, Vedantham V, von Drehle M, Muth AN, Tsuchihashi T, McManus MT, Schwartz RJ, Srivastava D (2007) Dysregulation of cardiogenesis, cardiac conduction, and cell cycle in mice lacking miRNA-1-2. Cell 129(2):303–317. https://doi.org/10.1016/j.cell.2007.03.030

Publisher's Note Springer Nature remains neutral with regard to jurisdictional claims in published maps and institutional affiliations.